Neurobiology of Disease 127 (2019) 53–64

Contents lists available at ScienceDirect

Neurobiology of Disease

journal homepage: www.elsevier.com/locate/ynbdi

Fragile X Mental Retardation Protein positively regulates PKA anchor Rugose and PKA activity to control actin assembly in learning/memory circuitry

James C. Sears[a], Woong Jae Choi[b], Kendal Broadie[c,*]

[a] Vanderbilt Brain Institute, Departments of Biological Sciences, Vanderbilt University and Medical Center, Nashville, TN 37235, USA
[b] Departments of Biological Sciences, Vanderbilt University and Medical Center, Nashville, TN 37235, USA
[c] Vanderbilt Brain Institute, Departments of Biological Sciences, Cell and Developmental Biology, and Pharmacology, Vanderbilt University and Medical Center, Nashville, TN 37235, USA

ARTICLE INFO

Keywords:
Fragile X syndrome (FXS)
Neurobeachin (NBEA)
A-Kinase Anchor Protein (AKAP)
Protein Kinase A (PKA)
Mushroom Body
Drosophila

ABSTRACT

Recent work shows Fragile X Mental Retardation Protein (FMRP) drives the translation of very large proteins (> 2000 aa) mediating neurodevelopment. Loss of function results in Fragile X syndrome (FXS), the leading heritable cause of intellectual disability (ID) and autism spectrum disorder (ASD). Using the *Drosophila* FXS disease model, we discover FMRP positively regulates the translation of the very large A-Kinase Anchor Protein (AKAP) Rugose (> 3000 aa), homolog of ASD-associated human Neurobeachin (NBEA). In the central brain Mushroom Body (MB) circuit, where Protein Kinase A (PKA) signaling is necessary for learning/memory, FMRP loss reduces Rugose levels and targeted FMRP overexpression elevates Rugose levels. Using a new *in vivo* transgenic PKA activity reporter (PKA-SPARK), we find FMRP loss reduces PKA activity in MB Kenyon cells whereas FMRP overexpression elevates PKA activity. Consistently, loss of Rugose reduces PKA activity, but Rugose overexpression has no independent effect. A well-established PKA output is regulation of F-actin cytoskeleton dynamics. In the FXS disease model, F-actin is aberrantly accumulated in MB lobes and single MB Kenyon cells. Consistently, Rugose loss results in similar F-actin accumulation. Moreover, targeted FMRP, Rugose and PKA overexpression all result in increased F-actin accumulation in the MB circuit. These findings uncover a FMRP-Rugose-PKA mechanism regulating actin cytoskeleton. This study reveals a novel FMRP mechanism controlling neuronal PKA activity, and demonstrates a shared mechanistic connection between FXS and NBEA associated ASD disease states, with a common link to PKA and F-actin misregulation in brain neural circuits.

Significance Statement: Autism spectrum disorder (ASD) arises from a wide array of genetic lesions, and it is therefore critical to identify common underlying molecular mechanisms. Here, we link two ASD states; Neurobeachin (NBEA) associated ASD and Fragile X syndrome (FXS), the most common inherited ASD. Using established *Drosophila* disease models, we find Fragile X Mental Retardation Protein (FMRP) positively regulates translation of NBEA homolog Rugose, consistent with a recent advance showing FMRP promotes translation of very large proteins associated with ASD. FXS exhibits reduced cAMP induction, a potent activator of PKA, and Rugose/NBEA is a PKA anchor. Consistently, we find brain PKA activity strikingly reduced in both ASD models. We discover this pathway regulation controls actin cytoskeleton dynamics in brain neural circuits.

1. Introduction

Fragile X Mental Retardation Protein (FMRP) is an mRNA-binding translation regulator that restricts synaptogenesis and refines synaptic connectivity in developing neural circuits (Davis and Broadie, 2017; Sears and Broadie, 2018). Recent work shows FMRP promotes translation of very large (> 2000 aa) proteins (Greenblatt and Spradling, 2018). The *Drosophila* Fragile X syndrome (FXS) model (*dfmr1* loss-of-function) has been instrumental in understanding FMRP functions, with human FMRP fully restoring disease phenotypes (Coffee et al., 2010). The *Drosophila* central brain Mushroom Body (MB) learning/memory center has been especially useful in linking FMRP translational control to neural circuit dynamics (Tessier and Broadie, 2011; Vita and Broadie, 2017), particularly during the early-use critical period

* Corresponding author.
E-mail address: kendal.broadie@vanderbilt.edu (K. Broadie).

https://doi.org/10.1016/j.nbd.2019.02.004
Received 8 December 2018; Accepted 4 February 2019
Available online 13 February 2019
0969-9961/

(0–2 days post-eclosion; dpe) when initial sensory input refines the MB circuit (Doll and Broadie, 2015, 2016; Doll et al., 2017). MB Kenyon cells (KCs) project into distinct axonal lobes (α/β, α'/β' and γ; Davis and Dauwalder, 1991; Skoulakis et al., 1993; Crittenden et al., 1998), with *dfmr1* null mutants exhibiting axon overgrowth and reduced pruning in the 0–2 dpe critical period (Pan et al., 2004; Tessier and Broadie, 2008).

The MB γ lobe has been a particular focus owing to established roles in learning and memory dependent on cyclic AMP (cAMP) – Protein Kinase A (PKA) signaling (Zars et al., 2000; Blum et al., 2009). Importantly, FXS patient cells and *Drosophila*/mouse disease models display reduced cAMP levels and cAMP induction (Berry-Kravis and Huttenlocher, 1992; Berry-Kravis et al., 1995; Kelley et al., 2007). Since cAMP activates PKA, these findings strongly imply that FMRP regulation on PKA could be a critical component disrupted in the FXS disease state. To assay PKA in the MB circuit, we employ a recently developed *in vivo* PKA activity sensor (PKA-SPARK; Zhang et al., 2018). PKA-SPARK is an eGFP-tagged chimeric protein reporter that is specifically phosphorylated by PKA to generate reversible phospho-oligomers visualized as fluorescent punctae (Zhang et al., 2018). PKA regulates actin cytoskeleton dynamics critical for neuronal growth and plasticity (Lin et al., 2005; Cingolani and Goda, 2008; Zhu et al., 2015). We therefore hypothesized that PKA misregulation in the FXS condition should result in defective F-actin assembly, which in turn would provide a mechanism for neuronal growth and plasticity defects.

We identify here the very large (> 3000 aa) Rugose protein as a target of FMRP positive translation regulation. Rugose is a brain-enriched protein that functions as an A-Kinase Anchor Protein (AKAP) required for normal MB-dependent learning/memory (Wang et al., 2000; Volders et al., 2012). AKAPs bind PKA to determine enzyme localization and activity (Smith et al., 2017; Wild and Dell'Acqua, 2017). Rugose and PKA catalytic subunit (PKA-C) genetically interact, with combined partial loss-of-function resulting in impaired memory dependent on MB γ lobe function (Zhao et al., 2013). Human Rugose homolog Neurobeachin (NBEA) is a similar, very large, brain-enriched protein associated with autism spectrum disorder (ASD; Wang et al., 2000; Castermans et al., 2003, 2010). Mammalian NBEA facilitates neuronal intracellular trafficking (Niesmann et al., 2011; Gromova et al., 2018), although AKAP function in this mechanism is uncertain (Wild and Dell'Acqua, 2017). Importantly, mammalian NBEA has been shown to be involved in F-actin cytoskeleton regulation (Niesmann et al., 2011). We therefore hypothesized that FMRP-dependent translation of Rugose/NBEA may be the pathway controlling PKA activity regulation of F-actin dynamics.

In this study, we show FMRP binds *rugose* mRNA, with Rugose protein decreased with FMRP loss and increased with FMRP overexpression in the MB circuit. Using PKA-SPARK, we find that MB-targeted FMRP loss reduces PKA activity, whereas FMRP overexpression increases PKA activity. Similarly, Rugose loss decreases PKA activity. Using phalloidin and LifeAct F-actin reporters, we find actin dynamics strikingly altered, with F-actin highly enriched in the FXS disease model. Consistent with a FMRP-Rugose-PKA pathway, FMRP, Rugose and PKA-C overexpression all result in F-actin accumulation within the MB γ lobe. Loss of *rugose* results in highly aberrant F-actin assembly similar to the FXS disease model. We conclude FMRP positively regulates translation of the AKAP Rugose/NBEA to modulate PKA signaling and control F-actin cytoskeleton dynamics in developing learning/memory circuitry.

2. Materials and methods

2.1. Drosophila genetics

All animals were maintained on a standard cornmeal/agar/molasses *Drosophila* food in a 12-h light:dark cycling incubator at 25 °C. All animals were staged as adults at 25 °C to 1-day post-eclosion (1 dpe). w^{1118} (BDSC 3605) was used as a genetic background control. Mutant lines used included the $dfmr1^{50M}$ null allele (Zhang et al., 2001) and the rg^{FDD} null allele (Volders et al., 2012). w^{1118} was outcrossed to control *elav*-GAL4 driver for rescue experiments, while Gal4 driver controls were outcrossed with control stocks P{y[+t7.7] = CaryP}attP2 (BDSC 36303) and P{y[+t7.7] = CaryP}attP40 (BDSC 36304). Transgenic Gal4 driver lines used: pan-neuronal *elav*-GAL4 (Coffee et al., 2010), the MB-selective OK107-Gal4 (BDSC 854; Connolly et al., 1996) and GMR-51C05-Gal4 (BDSC 47368; Jenett et al., 2012) expressing in two KCs innervating the MB γ lobe. Transgenic UAS responder lines used: wildtype UAS-$dfmr1^{9557–3}$ (Zhang et al., 2001), UAS-$dfmr1^{9557–3}$, $dfmr1^{50M}$ (Gatto and Broadie, 2009), UAS-*dfmr1* RNAi (BDSC 35200; Kashima et al., 2017; Greenblatt and Spradling, 2018), wildtype UAS-*rugose* (Volders et al., 2012), wildtype UAS-PKA-C (BDSC 35555; Kiger et al., 1999), UAS-PKA-C without catalytic activity (PKA-C K75A; BDSC 35559; Kiger and O'Shea, 2001), UAS-BRP-Short::mCherry (Fouquet et al., 2009), UAS responder line for PKA-*s*eparation of *p*hases-based *a*ctivity *r*eporter of *k*inase (UAS-PKA-SPARK; Zhang et al., 2018), and UAS-LifeAct::GFP (BDSC 58718; Huelsmann et al., 2013). Recombinant line GMR-51C05-Gal4, $dfmr1^{50M}$ was generated using standard genetic procedures, and female/male numbers were kept consistent between compared groups.

2.2. RNA immunoprecipitation

Studies were done as previously described (Zhang et al., 2001; Vita and Broadie, 2017). Briefly: 100 staged 1dpe heads from w^{1118} control and $dfmr1^{50M}$ null animals were homogenized in lysis buffer (20 mM HEPES, 100 mM NaCl, 2.5 mM EDTA, 0.05% Triton X, 5% glycerol, 1 × SigmaFast Protease inhibitor (Sigma S8820), 120 Units/mL Protector RNase inhibitor (Roche 03335399001), then incubated overnight at 4 °C with Dynabeads (Invitrogen 10003D) pre-conjugated to mouse anti-FMRP (Abcam 6A15) following the manufacturer's protocols. Bead-derived supernatant was then separated by TRIzol (Invitrogen 15596018) with Chloroform, and the upper aqueous layer transferred to a new tube. Glycogen and 2-propanol were added, the supernatant removed, and the resulting pellet washed with 75% EtOH, followed by centrifugation and air drying. 20 μL nuclease free water was added and the isolated RNA was reverse transcribed with the SuperScript Vilo kit (Invitrogen 11754-050). Similar protocols were used to isolate RNA from input lysates. cDNA was amplified with HotStart Taq (New England Biolabs M0495) using a touchdown PCR protocol, then amplified cDNA was separated on a 0.8% agarose gel and visualized with SYBR Safe DNA stain (Invitrogen S33102). Gels were imaged with a BIO-RAD Gel Doc EZ system. PCR primers used: *α-tubulin*; CTGTGGTCGATGAG GTCCG forward, GCGTAGGTCACCAGAGGG reverse. *futsch;* CAGTTTC ACCCGCCACCG forward, GCACGTTGCTGTTGTTTAGGC reverse. *rg*; CCAGCTACGCCGAATCGC forward, GGTCATCAGGTATTCACCATCGC reverse.

2.3. Western blots

Studies were done as previously described (Zhang et al., 2001; Vita and Broadie, 2017). Briefly, staged 1dpe heads were snap frozen on dry ice and homogenized in RIPA buffer containing 1 × Roche complete EDTA-free protease inhibitor (Roche 04693123001). Lysates were spun for 10 min at 4 °C, 16,000 × *g*, and protein amount was quantified by BCA. LDS (Invitrogen NP0007) and NuPAGE reducing (Invitrogen NP0009) agent were added to lysates, then samples were heated for 10 mins at 70 °C. Equal volumes of lysates from 2 brains were loaded per lane onto a 3–8% Tris-Acetate gel (Invitrogen EA0375) with tris-acetate running buffer (Invitrogen LA0041) and NuPAGE antioxidant (Invitrogen NP0005) in the upper buffer chamber. GE Healthcare Rainbow molecular weight marker (GE 45001591) and HiMARK pre-stained protein standard (Invitrogen LC5699) were used as ladders. Gels were run for 5 mins at 20 mA and then 30 mA for 1 h. Separated proteins

were transferred to nitrocellulose membranes overnight at 33 mA in 10% methanol in NuPAGE transfer buffer (NP0006) with NuPAGE antioxidant. To compare loading, protein was quantified with REVERT total protein stain (LI-COR 926–11010) on a LICOR Odyssey machine (Eaton et al., 2013). Membranes were blocked in 2% powdered skim milk in TBS-T overnight, incubated with primary antibodies in 2% powdered skim milk in TBS-T overnight, then incubated with fluorescently conjugated secondary antibodies in 2% powdered skim milk in TBS-T for 2 h at RT, all with rotation. Membranes were imaged using a LI-COR Odyssey machine. Protein bands were standardized to the total protein recording from the lane with the highest total protein levels. Primary antibodies used were: mouse anti-FMRP (1: 4000; Sigma 6A15; Wan et al., 2000; Zhang et al., 2001; Gatto and Broadie, 2009; Coffee et al., 2012; Doll and Broadie, 2015), rabbit anti-Rugose (1:2000; Volders et al., 2012). Secondary antibodies were Alexa Fluor 680 goat anti-rabbit (A-21076) and Alexa Fluor 680 goat anti-mouse (A-21048) and Rockland IRDye 800 anti-mouse (610-132-121), all at 1:10,000.

2.4. PKA assay

PKA activity was measured as *s*eparation of *p*hases-based *a*ctivity *r*eporter of *k*inase (PKA-SPARK) fluorescent punctae with live imaging (Zhang et al., 2018). PKA-SPARK uses 2 homo-oligomeric coiled coil transgenes: 1) a tetramer with phosphothreonine-binding domains (FHA1) and 2) a hexamer containing eGFP and a peptide sequence specifically phosphorylated by PKA (LRRATLVD) (Durocher et al., 2000; Woolfson et al., 2015). When threonine in the peptide sequence is phosphorylated by PKA, the domains associate to concentrate eGFP. Combined with the UAS/Gal4 system, PKA-SPARK can be driven in a cell-type selective manner (Zhang et al., 2018). UAS-PKA-SPARK is driven selectively in Kenyon cells with OK107-Gal4 (BDSC 854). Staged brains at 1 dpe were acutely dissected in 1× PBS and placed in Fluoromount (EMS 17984) between two #1 coverslips separated by a layer of tape for immediate imaging. Kenyon cell somata were imaged as stacks taken at slice widths of 3.5 µm at 3.5 µm intervals. Each slice was imaged at 5% 488 strength with a 0.8 µs pixel dwell time, line 2 averaging and 1024 × 1024 pixel resolution (0.22 µm × 0.22 µm xy pixel dimensions). Comparisons were made between groups using identical imaging settings. PKA-SPARK punctae were scored slice by slice with the Find Maxima feature in ImageJ using the same noise toleration setting between compared groups.

2.5. Immunocytochemistry imaging

For immunostaining, staged brains at 1 dpe were fixed in 4% PFA 1× PBS 4% sucrose for 30 min with rotation. Fixed brains were washed 3 times with 1× PBS then blocked for 1.5 h in blocking buffer (1× PBS, 1% BSA, 0.5% Goat Serum, 0.2% Triton X-100) with rotation. Brains were incubated with primary antibody overnight at 4 °C with rotation. Primary antibodies used were mouse anti-FMRP (6A15; Sigma 1:500; Abcam 1:62.5; Wan et al., 2000; Zhang et al., 2001; Gatto and Broadie, 2009; Coffee et al., 2012; Doll and Broadie, 2015), rat anti-Rugose (1:500; Volders et al., 2012), mouse anti-FasII (1:10; 1D4; Developmental Studies Hybridoma Bank), rabbit anti-RFP (1:2000; Rockland 600-401-379) and rabbit anti-GFP (1:4000; Abcam ab290). Brains were incubated with secondary antibodies for 2 h at RT with rotation. Fluorescent secondary antibodies used were Alexa Fluor 488 goat anti-mouse (A-11001), Alexa Fluor 555 donkey anti-mouse (A-31570), Alexa Fluor 568 goat anti-rabbit (A-11011), Alexa Fluor 488 goat anti-rabbit (A-11008) and Alexa Fluor 488 donkey anti-rat (A-21208), all at 1:500. To mark F-actin, Alexa Fluor 488-conjugated phalloidin (1:250; Invitrogen A12379) and BODIPY 558/568-conjugated phalloidin (1:500; Invitrogen B3475) were used for 2 h at RT with rotation. Stained brains were mounted in Fluoromount (EMS 17984) between two #1 coverslips separated by a layer of tape. All microscopy imaging was done on a Zeiss LSM 510 Meta confocal microscope using a Plan Neofluar 40× oil immersion objective with a numerical aperture of 1.3. Compared groups were stained simultaneously in the same tube when possible to control for staining variability and genotyped with antibody staining.

2.6. Data analyses

All statistical analyses were conducted using GraphPad Prism. All compared groups were processed in parallel at the same time and under the same conditions. All compared samples were imaged at identical settings, with image analysis conducted using ImageJ. FasII staining was used to identify the MB γ lobe for quantification, and to isolate the γ lobe from other MB lobes for projection analysis. Groups passing normality tests were compared with unpaired Welch's *t*-tests and unpaired ordinary one-way ANOVA with Tukey's multiple comparisons tests, for single and multiple comparisons respectively. Other groups were compared with Kruskal-Wallis tests and then Dunn's correction for multiple comparisons. Statistical significance is presented in figures as not significant (n.s.; $p > .05$), * $p < .05$, ** $p < .01$ and *** $p < .001$.

3. Results

3.1. FMRP promotes Rugose expression in Mushroom Body Kenyon cells

FMRP has been most widely characterized as a negative translation regulator (Laggerbauer et al., 2001; Li et al., 2001) and this is also true in the *Drosophila* FXS model, with elevated overall brain protein levels and increased translation of specific targets (Zhang et al., 2001; Tessier and Broadie, 2008). However, FMRP also has long been known to positively regulate the translation of other targets (Todd et al., 2003; Derlig et al., 2013) and FMRP was recently shown to generally promote translation of very large proteins with critical roles in neurodevelopment (Greenblatt and Spradling, 2018). In a candidate screen for proteins misregulated in the *Drosophila* FXS model brain (Tessier and Broadie, 2012), we identified the very large A-Kinase Anchoring Protein Rugose/NBEA (> 3000 aa; 460 kDa) (Volders et al., 2012) as a candidate FMRP target. Here we test this interaction with a combination of 1) RNA immunoprecipitation (RIP) using a well-characterized anti-FMRP antibody (Wan et al., 2000; Zhang et al., 2001; Vita and Broadie, 2017) to assay for *rugose* transcript binding, 2) Western blot studies of Rugose protein levels in the brain using a well-characterized anti-Rugose antibody (Volders et al., 2012), and 3) imaging studies of Rugose in the brain Mushroom Body (MB) learning/memory center using both FMRP loss-of-function (LOF) RNAi and MB-targeted gain-of-function (GOF) overexpression. Representative raw data and quantified results for these analyses are shown in Fig. 1.

To test FMRP interaction with *rugose* mRNA, we used RNA immunoprecipitation (RIP) to assay for *rugose* direct transcript binding (Zhang et al., 2001; Vita and Broadie, 2017). Lysates from newly-eclosed (1 dpe) w^{1118} genetic background control and *dfmr1* null mutant ($dfmr1^{50M}$) heads (100 heads/genotype) were incubated with a characterized anti-FMRP antibody conjugated to magnetic beads (Zhang et al., 2001; Vita and Broadie, 2017). The mRNA from head lysates was pulled down with the beads and isolated, reverse transcribed into cDNA, and then amplified with specific primers (see Methods). As previously, *futsch/map1b* was used as the positive control and *α-tubulin* as the negative control for FMRP binding (Zhang et al., 2001; Vita and Broadie, 2017). Specific primers for *rugose* mRNA were used to test anti-FMRP immunoprecipitation (Fig. 1A). In input lanes, strong bands representing PCR product amplified from all three mRNAs are present (Fig. 1A). In w^{1118} controls, but not in *dfmr1* null animals, there are strong bands for the *futsch* positive control (Fig. 1A). Bands for *α-tubulin* negative control are only observed in the input lanes, demonstrating FMRP-binding specificity (Fig. 1A). Controls also show a strong band for *rugose*, while *dfmr1* null animals do not, indicating that

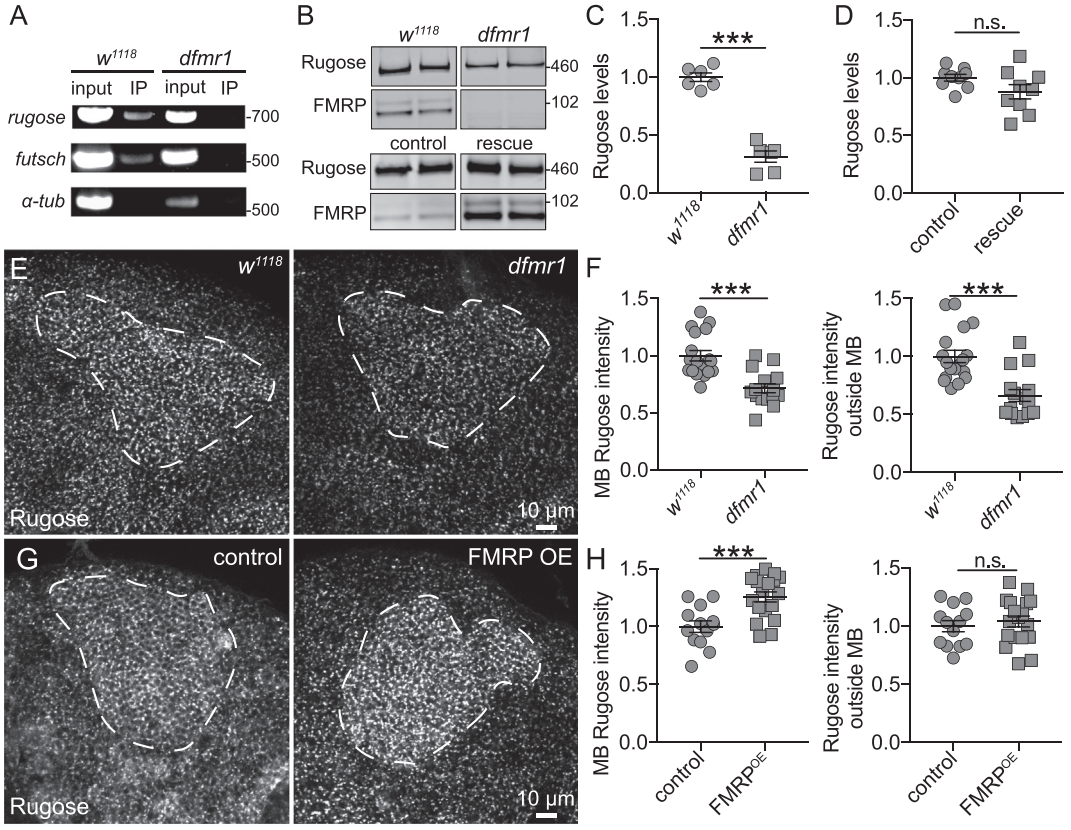

Fig. 1. FMRP promotes AKAP Rugose expression in the MB learning/memory circuit.
(A) RNA immunoprecipitation (RIP) comparing w^{1118} genetic background control and *dfmr1* null brains ($dfmr1^{50M}/dfmr1^{50M}$). Amplified cDNA transcribed from input lysates and RNA pulled down with anti-FMRP-conjugated Dynabeads; *futsch* is the positive control and *α*-tubulin is the negative control. Molecular weights are indicated to the right. (B) Western blots of control (w^{1118}) vs. *dfmr1* null ($dfmr1^{50M}$)(top), and driver control (*elav*-Gal4/+) vs. UAS-*dfmr1* rescue (*elav*-Gal4/+; UAS-$dfmr1^{9557\text{-}3}$, $dfmr1^{50M}/dfmr1^{50M}$) (bottom) brains at 1 day post-eclosion (1dpe). Proteins indicated on left, molecular weights on the right. (C-D) Dot plots of the normalized Rugose band intensities, showing the mean ± SEM. (E) Representative confocal images of anti-Rugose labeling in w^{1118} control and *dfmr1* null brains. Dashed lines separate MB Kenyon cell somata from surrounding brain tissue. (F) Dot plots of normalized Rugose intensity, showing mean ± SEM. (G) Representative confocal images of anti-Rugose labeling in MB-specific driver control (OK107-Gal4/+) and FMRP overexpression (OE) in MB (UAS-$dfmr1^{9557\text{–}3}$/+; OK107-G4/+). Dashed lines separate the MB Kenyon cell somata from surrounding brain tissue. (H) Dot plots of normalized Rugose intensity, showing mean ± SEM. Statistics were done with unpaired Welch's *t*-tests. Statistical significance is indicated as n.s. (not significant) and *** ($p < .001$).

rugose mRNA is bound by FMRP (Fig. 1A). In *dfmr1* null animals, bands are not observed in any of the anti-FMRP pulldowns, demonstrating assay specificity (Fig. 1A). Similar data from no antibody controls also confirm assay specificity (data not shown). These results show that FMRP directly binds *rugose* mRNA.

FMRP mRNA-binding has been shown to both suppress and promote translation of different specific targets (Zhang et al., 2001; Vita and Broadie, 2017; Derlig et al., 2013). Given the very large size of Rugose (MW 460 kDa), we hypothesized Rugose would be positively regulated by FMRP, consistent with similar very large proteins promoted by FMRP (Greenblatt and Spradling, 2018). Using Western blots, we tested total Rugose protein levels in *dfmr1* null mutants ($dfmr1^{50M}$) compared to the genetic background controls (w^{1118}) from isolated heads age-matched at 1 dpe (Fig. 1B). Lysates from w^{1118} heads show consistent, strong bands at ~460 kDa (Fig. 1B), comparable to published data (Volders et al., 2012). We find that Rugose levels are significantly reduced by ~70% in *dfmr1* null mutants compared to matched controls (normalized w^{1118} 1.0 ± 0.038 ($n = 6$) vs. $dfmr1^{50M}$ 0.312 ± 0.048 (n = 6); t(9.418) = 11.22, $p < .0001$, two-tailed Welch's *t*-test; Fig. 1C). Reintroduction of wildtype FMRP only in neurons using the *elav*-Gal4 driver in the otherwise *dfmr1* null background fully restores Rugose to the control levels (Fig. 1B). Quantification shows no significant difference persisting between genetic background control and the transgenic rescue (*elav*-Gal4/+ control 1.0 ± 0.029 ($n = 9$) vs. *dfmr1* rescue 0.879 ± 0.062 (n = 9); t(11.41) = 1.758, $p = .1055$, two-tailed Welch's *t*-test; Fig. 1D). Taken together, these data indicate that FMRP is necessary within brain neurons to promote Rugose translation.

Both FMRP and Rugose are specifically required in the Mushroom Body (MB) for olfactory learning and memory (Bolduc et al., 2008; Volders et al., 2012), with both proteins localized to the MB Kenyon cell (KC) somata. The two proteins show a high degree of spatial overlap and co-localization throughout the brain in neuron cell bodies (data not shown). Rugose labeling is punctate and highly enriched in KC somata, with significantly higher densities in KCs relative to surrounding brain tissue (KC 1.447 ± 0.065 ($n = 18$) vs. normalized adjacent brain 1.0 ± 0.053 (n = 18); t(32.67) = 5.323, $p < .0001$, two-tailed Welch's *t*-test; Fig. 1E). In comparing Rugose levels between *dfmr1* null mutants and age-matched control w^{1118} MB at 1 dpe, we find reduced Rugose labeling both in and around the KC somata (Fig. 1E). Quantitatively, we find a ~30% decrease in Rugose labeling intensity within the KC somata in null mutants compared to controls (normalized w^{1118} 1.0 ± 0.045 (n = 18) vs. $dfmr1^{50M}$ 0.715 ± 0.040 ($n = 15$); t(30.97) = 4.754 p < .0001, two-tailed Welch's *t*-test; Fig. 1F, left). Similarly, we observe in *dfmr1* null animals an approximately ~30% decrease in staining intensity outside of the Kenyon cells (w^{1118} 1.0 ± 0.053 (n = 18) vs. $dfmr1^{50M}$ 0.664 ± 0.052 (n = 15); t(30.86) = 4.542, $p < .0001$, two-tailed Welch's *t*-test; Fig. 1F, right). We conclude that loss of FMRP results in reduced Rugose levels in KC somata and surrounding neuronal cell bodies of the brain.

We next tested if FMRP overexpression (OE) would cause the opposite change. Using MB-specific OK107-Gal4 to drive UAS-FMRP (Connolly et al., 1996; Zhang et al., 2001), we find strong enrichment of Rugose specifically in the KC somata (Fig. 1G). Quantitatively, we find a ~25% increase in Rugose levels (normalized control 1.0 ± 0.050 (n = 13) vs. FMRP^{OE} 1.256 ± 0.044 (n = 18); t(26.62) = 3.876, p = .0006, two-tailed Welch's t-test; Fig. 1H, left). This increase is specific to KCs overexpressing FMRP, since Rugose levels in adjacent brain areas are not significantly different compared with controls (control 1.0 ± 0.048 (n = 13) vs. FMRP^{OE} 1.04 ± 0.047 (n = 18); t(27.89) = 0.596, p = .5560, two-tailed Welch's t-test; Fig. 1H, right). Only OK107-Gal4 > UAS-FMRP animals display significantly elevated ratios of Rugose in KCs vs. adjacent cells. All other genotypes exhibit similar KC Rugose enrichment normalized to adjacent brain tissue (w^{1118}, 1.463 ± 0.038 (n = 18); $dfmr1^{50M}$ 1.597 ± 0.057 (n = 15); and OK107-Gal4/+, 1.50 ± 0.066 (n = 13)). In contrast, MB-targeted FMRP^{OE} causes a significantly increased ratio (1.813 ± 0.039 (n = 18), F = 11.52, p < .0001, w^{1118} vs. FMRP^{OE}, p = .0113, $dfmr1^{50M}$ vs. FMRP^{OE}, p = .0002, control vs. FMRP^{OE}, one-way ANOVA with Tukey's multiple comparisons test). Taken together, we conclude that FMRP is necessary for normal Rugose expression in Kenyon cells, and FMRP overexpression is sufficient to increase Rugose levels specifically in targeted Kenyon cells.

3.2. FMRP and Rugose both promote PKA activity in Mushroom Body Kenyon cells

Rugose is an A-Kinase Anchor Protein (AKAP) enriched in brain neurons (Wang et al., 2000; Volders et al., 2012), which genetically interacts with Protein Kinase A catalytic subunit (PKA-C) (Zhao et al., 2013). AKAPs have been demonstrated to bind PKA to determine localization and enzymatic activity (Smith et al., 2017). We therefore hypothesized that FMRP translational control of Rugose should regulate PKA dynamics in the MB circuit. To test this hypothesis, we used a recently developed transgenic PKA activity sensor (PKA-SPARK), an eGFP chimera that when phosphorylated by PKA forms reversible oligomers visualized *in vivo* as fluorescent punctae with live imaging (Zhang et al., 2018). We used MB-specific OK107-Gal4 driver to target UAS-PKA-SPARK and additional LOF/GOF constructs to KCs. Brains acutely dissected at 1dpe were immediately imaged for native eGFP fluorescence. To verify the PKA activity reporter specificity, we used OK107-Gal4 to target overexpression (OE) of the PKA catalytic subunit (PKA-C; Kiger et al., 1999) in the MB circuit. Transgenic controls exhibit small PKA-SPARK punctae compared to the much larger/brighter punctae with PKA overexpression (Fig. 2A). Quantification shows a 2.5-fold increase (normalized control 1.0 ± 0.092 (n = 6) vs. PKA-C^{OE} 2.537 ± 0.117 (n = 7); t(10.77) = 10.34, p < .0001, unpaired Welch's t-test; Fig. 2B), a highly significant elevation compared to controls. These results confirm the PKA-SPARK activity reporter.

We next tested PKA-SPARK with the MB-specific OK107-Gal4 driver targeting a characterized UAS-*dfmr1* RNAi (Kashima et al., 2017; Greenblatt and Spradling, 2018). In transgenic controls, PKA-SPARK punctae are largely restricted to the KC somata, less frequently in MB calyx dendritic arbors and rarely in the axonal lobes (Fig. 2C). With FMRP knockdown, PKA-SPARK punctae in the MB circuit are very obviously reduced in both abundance and fluorescence intensity (Fig. 2C). Quantification shows a striking ~60% loss of the PKA-SPARK punctae (normalized control 1.0 ± 0.040 (n = 18) vs. *dfmr1* RNAi 0.344 ± 0.025 (n = 21); t(28.73) = 13.84, p < .0001, Welch's unpaired t-test; Fig. 2D). We conclude that FMRP is necessary to promote PKA enzymatic activity in the MB KCs. To test whether FMRP is also limiting PKA activity in KCs, we next tested the PKA-SPARK sensor with the MB-specific OK107-Gal4 driver targeting a characterized UAS-*dfmr1* overexpression (OE) line (UAS-$dfmr1^{9557-3}$; Zhang et al., 2001). Compared to the transgenic control, we find a 2-fold increase in the number of PKA-SPARK fluorescent punctae in MBs overexpressing FMRP (normalized control 1.0 ± 0.024 (n = 24) vs. FMRP^{OE} 2.068 ± 0.112 (n = 26); t(27.23) = 9.31, p < .0001, unpaired Welch's t-test; Fig. 2E,F), a highly significant elevation. Taken together, these results demonstrate that FMRP is both necessary and sufficient to promote PKA activity in the Mushroom Body Kenyon cells.

We hypothesized FMRP regulates PKA activity via positive control of Rugose, and therefore loss of Rugose should similarly result in reduced PKA activity. To test this hypothesis, we used the characterized null allele rg^{FDD} (Volders et al., 2012), together with the PKA-SPARK reporter driven with MB-specific OK107-Gal4. The null mutants (rg^{FDD}/Y) exhibit a clear loss of PKA-SPARK fluorescent punctae in the MB compared to matched controls (Fig. 2G). Note a small subset of null brains (~20%) exhibit small KC populations (~15–40 cells) with aberrantly bright PKA-SPARK punctae. Nonetheless, quantification shows ~35% loss of PKA-SPARK punctae (normalized control 1.0 ± 0.038 (n = 15) vs. rg^{FDD}/Y 0.654 ± 0.043 (n = 20); t(32.97) = 6, p < .0001, Welch's t-test; Fig. 2H). We conclude Rugose overall promotes PKA enzymatic activity in MB KCs, consistent with AKAP function. To test whether Rugose is also limiting PKA activity, we next tested MB-specific OK107-Gal4 driving a characterized UAS-*rugose* overexpression (OE) line (UAS-*rg*; Volders et al., 2012). PKA activity is normal, consistent with previous reports of Rugose OE (Fig. 2I; Volders et al., 2012). Quantification shows no significant effect from Rugose overexpression (normalized control 1.0 ± 0.060 (n = 11) vs. Rugose^{OE} 0.894 ± 0.047 (n = 8); t(16.92) = 1.398, p = .180, unpaired Welch's t test; Fig. 2J). Taken together, these results demonstrate for the first time a direct effect of FMRP on PKA activity in neurons *in vivo* and establish a pathway by which FMRP regulates PKA activity through the large AKAP Rugose in the MB Kenyon cells.

3.3. FMRP regulates F-actin assembly in Mushroom Body Kenyon cells

Established FMRP targets have led to a focus on misregulated actin cytoskeleton (Michaelsen-Preusse et al., 2018). Importantly, PKA function is well known to regulate actin polymerization dynamics and particularly filamentous (F)-actin assembly during developmental neuronal growth as well as later activity-dependent plasticity (Lin et al., 2005; Cingolani and Goda, 2008; Zhu et al., 2015). We therefore hypothesized that the above striking defects in PKA activity in *dfmr1* null MB Kenyon cells would cause altered actin cytoskeleton dynamics and an aberrant F-actin array in the FXS disease model. To test this hypothesis, we first assayed the MB circuit at 1 dpe using fluorescently conjugated phalloidin as a specific F-actin marker (Melak et al., 2017). In wildtype animals, the MB exhibits strong F-actin phalloidin labeling within the MB calyx and α/β axon lobe cores, as reported previously (Abe et al., 2014; Doll et al., 2017). Moreover, we find that MB γ lobe F-actin phalloidin labeling is strongly increased relative to the surrounding neuropils (Fig. 3A). Given this accessible γ lobe labeling, we focused particularly on this location to assess changes in the F-actin cytoskeleton in the FXS disease model. For single cell resolution, we also employed the highly selective R51C05-Gal4 that expresses in just a couple MB γ lobe KCs (Jenett et al., 2012) to drive expression of the specific F-actin marker UAS-LifeACT (Melak et al., 2017). Representative images and quantified results are shown in Fig. 3.

In w^{1118} genetic background controls, phalloidin weakly labels MB KC somata, mostly around the periphery of the cell bodies. In contrast, MB neuropils have much stronger phalloidin labeling, demonstrating increased relative F-actin levels (Fig. 3A). In particular, the MB γ lobe displays especially strong phalloidin labeling, most prominently in the distal half of the lobe (Fig. 3A). Null *dfmr1* mutants ($dfmr1^{50M}$) display higher phalloidin labeling, with a striking increase in F-actin in the MB lobes relative to w^{1118} genetic background controls, particularly in the γ lobe (Fig. 3A, middle). This increase allows the γ lobe to be clearly delineated from surrounding brain tissue. Quantification shows ~40% increase in phalloidin fluorescence intensity in null animals compared with matched controls (normalized w^{1118} 1.0 ± 0.025 (n = 68) vs.

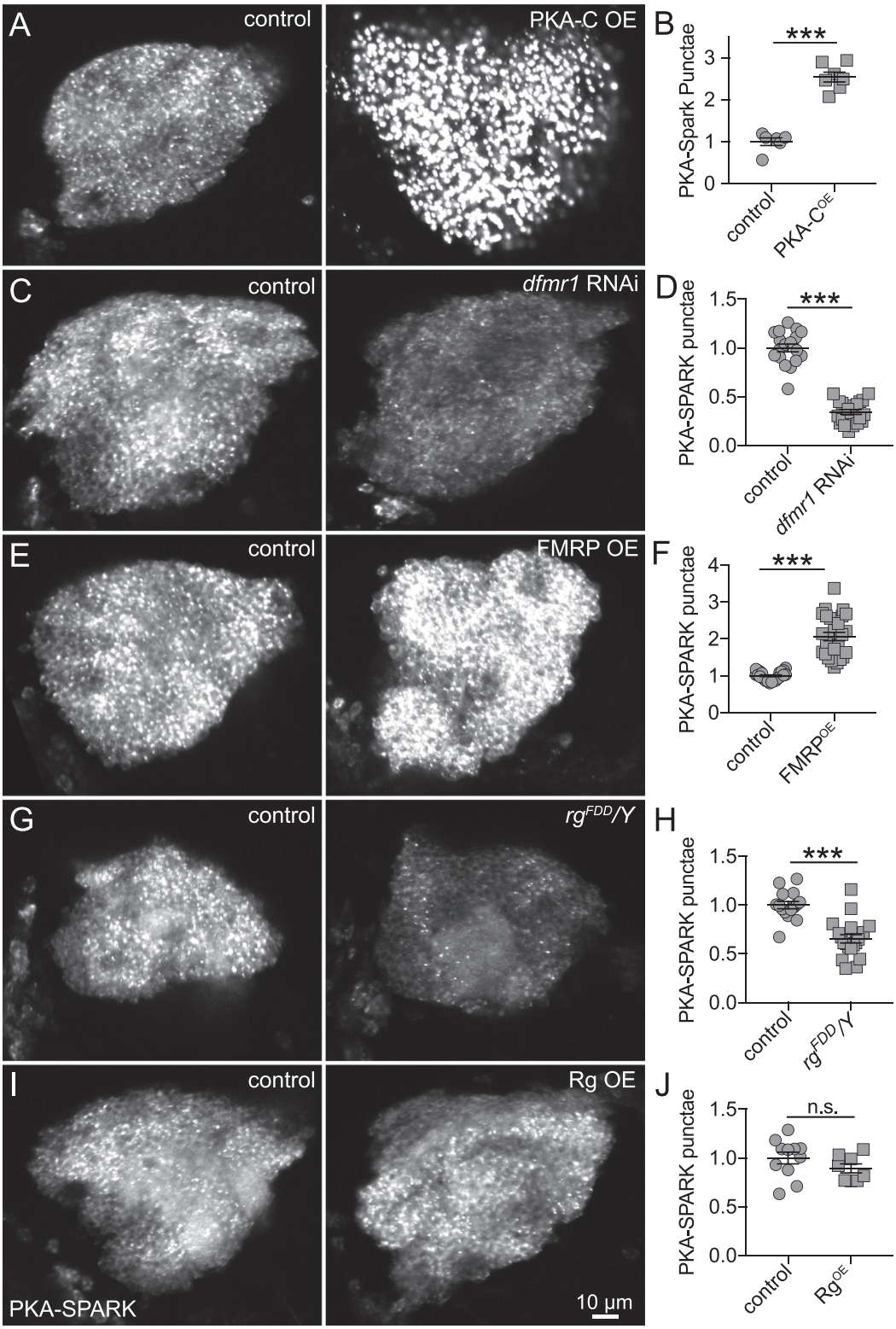

Fig. 2. FMRP and Rugose promote PKA activity in the MB learning/memory circuit. (A) Representative confocal images of MB Kenyon cells at 1 dpe in animals with OK107-Gal4 driving PKA activity sensor PKA-SPARK in the MB in the control genetic background (control, left) and with MB overexpression of the PKA catalytic subunit (UAS-PKA-C, right). (B) Dot plots of normalized PKA-SPARK punctae, with mean ± SEM. (C) Representative images of OK107-Gal4 driving PKA-SPARK alone (control, left) and driving PKA-SPARK and UAS-*dfmr1* RNAi (right). (D) Dot plots of normalized PKA-SPARK punctae, with mean ± SEM. (E) Representative images of OK107-Gal4 driving PKA-SPARK alone (control, left) and driving PKA-SPARK and FMRP overexpression (UAS-$dfmr1^{9557-3}$, right). (F) Dot plots of normalized PKA-SPARK punctae, with mean ± SEM. (G) Representative images of OK107-Gal4 driving PKA-SPARK in the control genetic background (control, left) and driving PKA-SPARK in the *rugose* null background (rg^{FDD}/Y, right). (H) Dot plots of normalized PKA-SPARK punctae, with mean ± SEM (I) Representative images of OK107-Gal4 driving PKA-SPARK alone (control, left) and driving PKA-SPARK and Rugose overexpression (UAS-*rg*, right). (J) Dot plots of normalized PKA-SPARK punctae with mean ± SEM. Statistics were done with unpaired Welch's *t*-tests. Statistical significance is indicated as n.s. (not significant) and *** ($p < .001$).

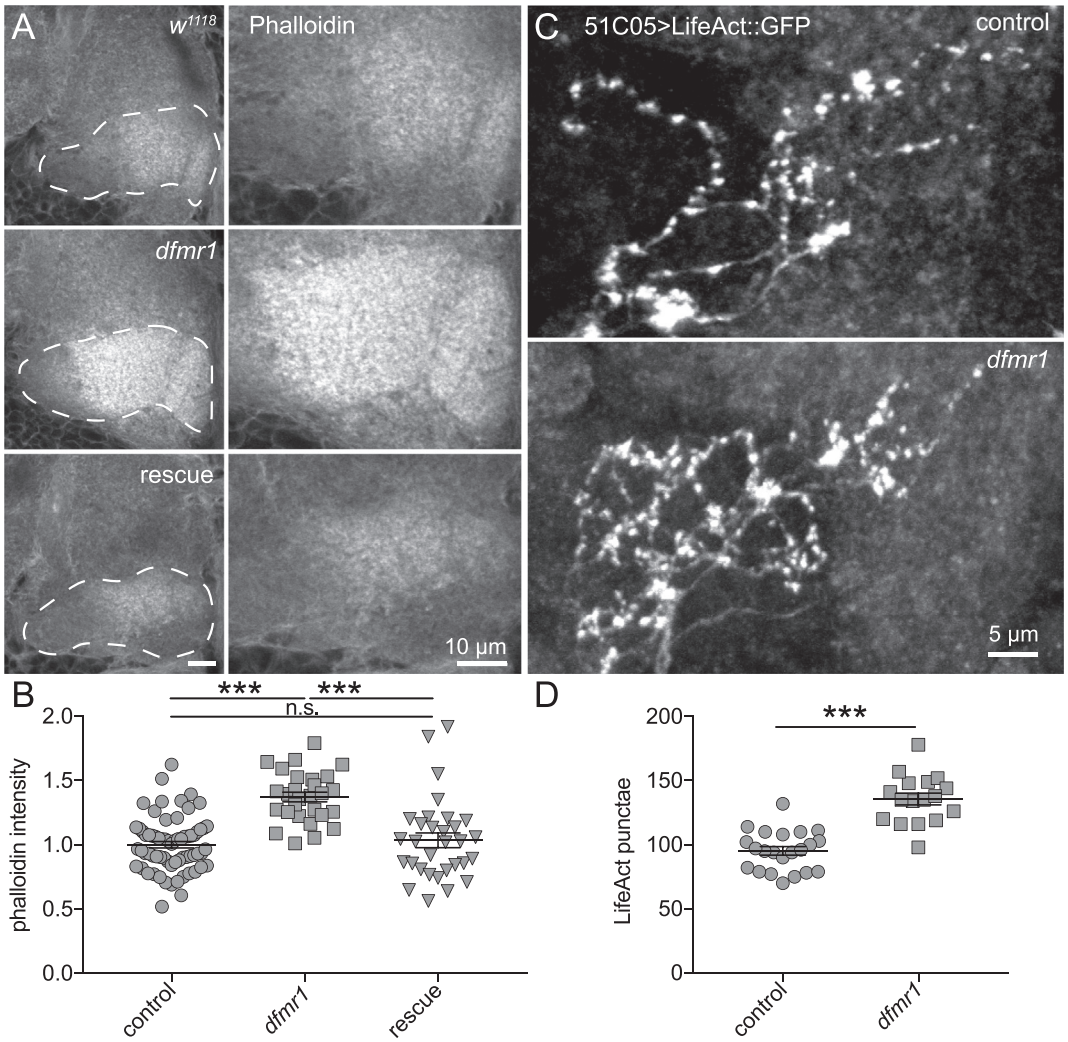

Fig. 3. FMRP limits F-actin cytoskeleton assembly in the MB learning/memory circuit. (A) Representative brain confocal images at 1 dpe of MB γ lobes (dashed outline) labeled with F-actin marker fluorescently-conjugated phalloidin. Right panels show higher magnification. Genotypes shown: genetic background control (w^{1118}, top), *dfmr1* null mutant ($dfmr1^{50M}/dfmr1^{50M}$, middle) and neuronal expression of wildtype FMRP in *dfmr1* null background (elav-Gal4/+; UAS-$dfmr1^{9557-3}$, $dfmr1^{50M}/dfmr1^{50M}$)(rescue, bottom). (B) Dot plots of normalized phalloidin intensity in the MB γ lobes, with mean ± SEM. (C) Representative brain confocal images of MB γ lobe projections expressing F-actin marker LifeAct driven by the selective KC driver R51C05-Gal4 in a transgenic control (UAS-LifeAct::GFP/+; R51C05-Gal4/+, top) and the *dfmr1* null mutants (UAS-LifeAct::GFP/+; R51C05-Gal4, $dfmr1^{50M}/dfmr1^{50M}$, bottom). (D) Quantification of LifeAct::GFP punctae, with mean ± SEM. Statistics were done with Kruskal-Wallis test with Dunn's correction for multiple comparisons (B) and unpaired Welch's *t*-test (D). Statistical significance is indicated as n.s. (not significant) and *** ($p < .001$).

$dfmr1^{50M}$ 1.372 ± 0.037 ($n = 28$)), a highly significant elevation of F-actin assembly ($p < .0001$, Kruskal-Wallis test with Dunn's multiple comparisons test; Fig. 3B). Phalloidin intensities of MB γ lobe projections isolated from the surrounding tissue exhibit a consistent ~35% increase in phalloidin intensity in *dfmr1* nulls compared to controls, likewise demonstrating a highly significant elevation (normalized w^{1118} 1.0 ± 0.023 (n = 68) vs. $dfmr1^{50M}$ 1.352 ± 0.037 (n = 28); $p < .0001$, Kruskal-Wallis test with Dunn's multiple comparisons test). These findings show highly elevated F-actin assembly in the FXS disease model within the Mushroom Body Kenyon cells.

To confirm the actin defect specificity, wildtype FMRP was re-introduced into neurons in a *dfmr1* null background (Doll and Broadie, 2015; Vita and Broadie, 2017). Neuronal *elav*-Gal4 driving UAS-$dfmr1^{9557-3}$ fully suppresses elevated phalloidin labeling in the MB γ lobe (Fig. 3A, bottom). Quantification shows no significant difference to the matched control (normalized rescue intensity 1.035 ± 0.057 ($n = 31$) and isolated lobes 0.990 ± 0.044 ($n = 32$); $p > .9$ vs. w^{1118} and $p < .0001$ vs. $dfmr1^{50M}$; Fig. 3B). To confirm increased phalloidin labeling is due to F-actin assembly in KCs, we used R51C05-Gal4 to drive the LifeAct::GFP F-actin marker (Huelsmann et al., 2013; Melak et al., 2017; Fig. 3C). In transgenic controls, LifeAct shows F-actin accumulated in varicosities along KC axons resembling synaptic boutons (Fig. 3C, top). We confirmed presynaptic Brp-short (Fouquet et al., 2009; Vasmer, 2016) mimics the LifeAct pattern (data not shown). Null *dfmr1* KCs display clearly increased LifeAct::GFP punctae compared to matched transgenic controls (Fig. 3C, bottom). Quantification shows increased LifeACT labeling, ~40% elevated in *dfmr1* nulls (control, 95.27 ± 3.32 punctae ($n = 22$) vs. $dfmr1^{50M}$, 135.6 ± 4.602 punctae ($n = 17$)), a highly significant elevation of F-actin assembly ($t(30.66) = 7.115$, $p < .0001$, unpaired Welch's *t*-test; Fig. 3D). We conclude that MB neurons in the FXS model exhibit increased F-actin. Given the role of Rugose and PKA downstream of FMRP, we next tested the FMRP-Rg-PKA pathway control of F-actin dynamics in the MB γ lobe.

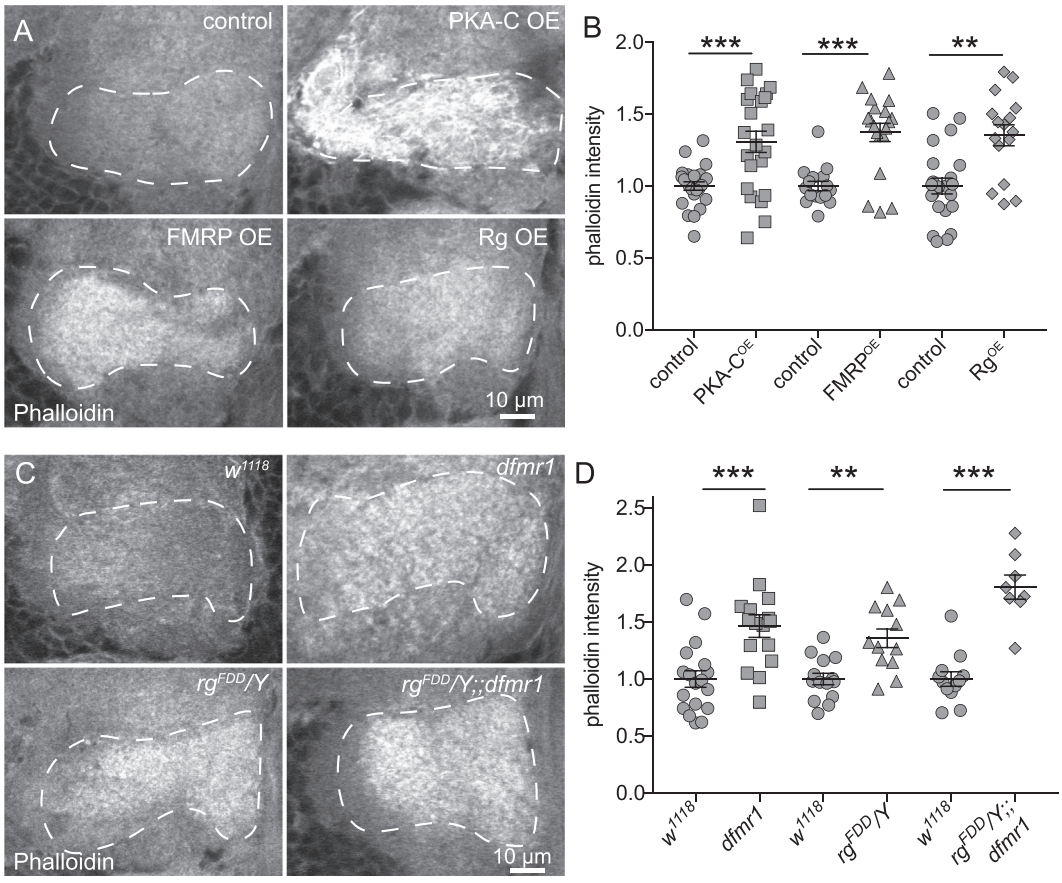

Fig. 4. PKA-C, FMRP and Rugose overexpression drive F-actin assembly in the MB, and Rugose reduction phenocopies the F-actin assembly defect in the FXS disease model. (A) Representative brain confocal images at 1 dpe of MB γ lobes (dashed outline) labeled with F-actin marker fluorescently-conjugated phalloidin for MB transgenic driver alone (OK107-Gal4/+ control, top left), targeted PKA-C overexpression (UAS-PKA-C/+; OK107-Gal4/+, top right), targeted FMRP overexpression (UAS-*dfmr1*$^{9557\text{-}3}$/+; OK107-Gal4/+, bottom left) and targeted Rugose overexpression (UAS-*rg*/+; OK107-Gal4/+, bottom right). (B) Dot plots of normalized phalloidin intensity in the MB γ lobe, with mean ± SEM. (C) Representative images of genetic background control (*w*^{1118}, top left), *dfmr1* null mutant (*dfmr1*^{50M}/*dfmr1*^{50M}, top right), *rugose* null (*rg*^{FDD}/*Y*, bottom left) and *rugose* null in *dfmr1* null background (*rg*^{FDD}/*Y;; dfmr1*^{50M}/*dfmr1*^{50M}, bottom right). (D) Dot plots of normalized phalloidin intensity in the MB γ lobe, with mean ± SEM. Statistics done with unpaired Welch's *t*-tests. Statistical significance is indicated as either ** ($p < .01$) or *** ($p < .001$).

3.4. Gain of FMRP, Rugose and PKA all drive F-actin assembly in the Mushroom Body

Our working hypothesis is that FMRP regulation of Rugose controls PKA activity to modulate F-actin dynamics. We reasoned that elevated PKA function should enhance F-actin assembly, consistent with a similar effect of FMRP overexpression. To test this hypothesis, we first used MB-specific OK107-Gal4 to drive UAS-PKA-C (Kiger et al., 1999) with phalloidin to label F-actin (Melak et al., 2017). With elevated PKA-C, F-actin becomes highly enriched in MB lobes, including the γ lobe (Fig. 4A, top). Indeed, the F-actin accumulation is so striking that the genotype can be easily identified with widefield microscopy. Quantification shows that driving PKA-C in the MB results in ~30% increase in MB γ lobe phalloidin labeling (normalized control 1.0 ± 0.030 ($n = 24$) vs. PKA-C^{OE} 1.308 ± 0.074 (n = 22)), a highly significant elevation of F-actin assembly (t(27.65) = 3.88, $p = .0006$, unpaired Welch's *t*-test; Fig. 4B). Similarly, isolated γ lobe projections show a significant ~25% increase in F-actin (control 1.0 ± 0.022 (n = 24) vs. PKA-C^{OE} 1.241 ± 0.071 (n = 22); t(25.15) = 3.258, $p = .0032$). The effect is specific to increased PKA catalytic activity, since driving PKA-C with a mutated catalytic subunit (PKA-C^{K75A}; Kiger and O'Shea, 2001) has no effect on F-actin phalloidin labeling in the MB γ lobe (normalized control intensity 1.0 ± 0.040 ($n = 12$) and isolated projection 1.0 ± 0.031 (n = 12) vs. PKA-C^{K75A} OE 0.931 ± 0.040 ($n = 14$) and 0.985 ± 0.026 (n = 14); t(23.79) = 1.217 and t(22.79) = 0.374, $p = .2355$ and 0.712, unpaired Welch's *t*-tests). We conclude that PKA activity positively regulates F-actin assembly in the MB axonal lobes.

Since driving FMRP in the MB results in enhanced PKA activity, we hypothesized F-actin would also be increased with FMRP overexpression. We tested this hypothesis using OK107-Gal4 to drive UAS-*dfmr1*$^{9557–3}$. Elevated FMRP results in ~40% increase in phalloidin labeling in the MB γ lobe (control 1.0 ± 0.033 ($n = 16$) vs. FMRP^{OE} 1.37 ± 0.064 ($n = 19$); t(26.77) = 5.188, $p < .0001$, unpaired Welch's *t*-test, Fig. 4A,B). Likewise, isolated γ lobe projections increase ~35% with elevated FMRP (control 1.0 ± 0.028 (n = 16) vs. FMRP^{OE} 1.354 ± 0.064 (n = 19); t(24.55) = 5.057, p < .0001, unpaired Welch's *t*-test). We conclude excess FMRP enhances F-actin assembly, consistent with PKA phenotypes. The hypothesized link is FMRP upregulation of Rugose translation, predicting Rugose overexpression should also increase F-actin assembly. We tested this hypothesis using OK107-Gal4 to drive UAS-*rugose*. Consistent with the prediction, Rugose elevation increases F-actin labeling in the MB γ lobe (Fig. 4A, bottom). Quantification shows Rugose OE results in ~30% increase in phalloidin intensity (control 1.0 ± 0.053 (n = 22) vs. Rugose^{OE} 1.286 ± 0.065 (n = 16)), indicating a highly significant elevation in F-actin (t(31.64) = 3.408, $p = .0018$, unpaired Welch's *t*-test; Fig. 4B). Consistently, isolated MB γ lobe projections show a significant increase in F-actin accumulation (normalized control 1.0 ± 0.039 (n = 22) vs. Rugose^{OE} 1.143 ± 0.051 (n = 16); t(30.35) = 2.231, $p = .033$, unpaired Welch's *t*-test). These results show that elevation in the level of

FMRP, Rugose and PKA all similarly increase F-actin assembly within the MB circuit.

3.5. Rugose reduction phenocopies F-actin assembly observed in FXS disease model

The above studies have established a consistent pathway of FMRP promoting Rugose translation to enhance PKA enzymatic activity in the MB learning/memory circuit, and thus upregulating F-actin assembly dynamics in the MB Kenyon cells. Importantly, note that both FMRP gain and loss result in increased F-actin assembly in this brain circuit. Consistently, it has been suggested that a "Goldilocks zone" can exist in mechanoaccumulation of F-actin, dependent on an appropriate level of binding affinity to both grant access to actin cross-linkers, and to enable actin binding efficacy (Schiffhauer et al., 2016). In the case of FMRP, our results show that too little or too much protein function affects F-actin assembly in the MB circuit. Since we propose FMRP regulates Rugose translation to control neuronal F-actin dynamics, we hypothesize that loss of Rugose should result in increased F-actin accumulation. Moreover, we predict that loss of both FMRP and Rugose would also result in increased F-actin accumulation. To test these hypotheses, we implemented a *rugose* null allele (rg^{FDD}), with and without the $dfmr1^{50M}$ allele (Zhang et al., 2001; Volders et al., 2012).

As established above (Fig. 3), we found again F-actin highly accumulated in the FXS model compared with the control background (Fig. 4C). Quantitatively, we observe ~45% increase in MB γ lobe phalloidin intensity in *dfmr1* nulls (normalized w^{1118} 1.0 ± 0.072 ($n = 18$) vs. $dfmr1^{50M}$ 1.464 ± 0.099 (n = 16)), showing a highly significant F-actin elevation (t(28.264) = 3.795, $p = .0007$, unpaired Welch's *t*-test; Fig. 4C,D). Consistently, isolated MB γ lobe projections show a significant increase in F-actin accumulation (normalized control 1.0 ± 0.048 (n = 18) vs. $dfmr1^{50M}$ 1.398 ± 0.091 (n = 16); t(22.845) = 3.867, $p = .0008$, unpaired Welch's *t*-test). The rg^{FDD}/Y hemizgous null animals also exhibit higher phalloidin intensities compared with controls, indicating that loss of *rugose* results in increased F-actin accumulation (Fig. 4C). In quantified comparisons, *rg* nulls show significantly increased intensity (normalized w^{1118} 1.0 ± 0.050 (n = 14) vs. rg^{FDD}/Y 1.357 ± 0.082 ($n = 12$); t(18.548) = 3.693, $p = .0016$, unpaired Welch's *t*-test; Fig. 4C,D). Isolated MB γ lobe projections show a similar result (normalized w^{1118} 1.0 ± 0.052 (n = 14) vs. rg^{FDD}/Y 1.223 ± 0.063 (n = 12); t(22.34) = 2.725, $p = .0123$, unpaired Welch's *t*-test). We next tested if animals lacking *rugose* (rg^{FDD}/Y) in an otherwise *dfmr1* null background ($dfmr1^{50M}/dfmr1^{50M}$) display alterations in F-actin assembly in the MB circuit. Similar to the single mutant allele backgrounds, we find that double mutants ($rg^{FDD}/Y;; dfmr1^{50M}/dfmr1^{50M}$) display elevated phalloidin labeling distribution and intensity compared with controls (Fig. 4C). Quantitatively, the double mutants show significantly increased MB γ lobe phalloidin (normalized w^{1118} 1.0 ± 0.0642 (n = 12) vs. $rg^{FDD}/Y;;dfmr1^{50M}/dfmr1^{50M}$ 1.806 ± 0.106 ($n = 8$); t(12.025) = 6.498, $p < .0001$, unpaired Welch's *t*-test, Fig. 4C,D). Similarly, isolated MB γ lobe projections display elevated phalloidin intensities (normalized w^{1118} 1.0 ± 0.0641 (n = 12) vs. $rg^{FDD}/Y;;dfmr1^{50M}/dfmr1^{50M}$ 1.853 ± 0.095 (n = 8); t(13.066) = 7.43, $p < .0001$, unpaired Welch's *t*-test). These data support the conclusion that loss of Rugose mediates the F-actin assembly defect characterizing the FXS disease model.

4. Discussion

Fragile X syndrome (FXS) is a very common intellectual disorder with high ASD comorbidity characterized by neuronal overelaboration linked to cytoskeletal dysfunction (Verkerk et al., 1991; Comery et al., 1997; Tessier and Broadie, 2008; Hunter et al., 2014; Michaelsen-Preusse et al., 2018). Fragile X Mental Retardation Protein (FMRP) is a mRNA-binding translation regulator of proteins including trafficking and cytoskeletal regulators (Davis and Broadie, 2017; Sears and Broadie, 2018). Using the *Drosophila* FXS model to search for novel FMRP targets, we found Rugose (Wang et al., 2000), the *Drosophila* homolog of ASD-linked Neurobeachin (NBEA; Castermans et al., 2003). Similar to the FXS condition, NBEA haploinsufficiency causes ASD-like features in mice and Rugose loss causes learning/memory deficits in *Drosophila* (Volders et al., 2012; Nuytens et al., 2013). Thus, this discovery connects these two ASD/ID disease states. We demonstrate here that FMRP binds *rugose* mRNA to positively regulate translation of the very large Rugose protein (460 kDa), with reduced expression in the FXS model brain. This discovery agrees with recent work showing FMRP promotes the translation of very large ASD-linked proteins (Greenblatt and Spradling, 2018).

In FXS patients and mouse/*Drosophila* disease models, loss of FMRP is mostly associated with elevated translation and increased protein levels (Zhang et al., 2001; Zalfa et al., 2003; Darnell et al., 2011; Jacquemont et al., 2018). However, FMRP has also been demonstrated to promote the translation of certain proteins involved in actin regulation and synaptic organization (Todd et al., 2003; Derlig et al., 2013, 2014). Recent ribosome profiling work shows FMRP enhances translation of very large (> 2000 aa) proteins (Greenblatt and Spradling, 2018). Consistently, the current study shows that the very large (> 3000 aa) Rugose protein is likewise positively regulated by FMRP. Moreover, mRNA-binding screens demonstrate mammalian FMRP likewise directly binds the Rugose homolog Neurobeachin (Wang et al., 2000; Darnell et al., 2011). Rugose/NBEA localize in the neuronal soma near the *trans*-Golgi network to regulate neuronal intracellular trafficking (Niesmann et al., 2011; Volders et al., 2012), based on ectopic F-actin accumulations near the Golgi and synaptic trafficking defects in mutants (Castermans et al., 2010; Nair et al., 2013). Consistently, the current study shows FMRP co-localized with Rugose in the neuronal soma drives Rugose translation to modulate F-actin accumulation in distal axons and synapses.

Consistent with FMRP positive regulation of Rugose, loss of either FMRP or Rugose similarly reduces PKA activity in the *Drosophila* Mushroom Body (MB) circuit, which mediates PKA-dependent learning/memory (Zars et al., 2000; Blum et al., 2009). This discovery was enabled with the just developed transgenic *in vivo* PKA activity sensor PKA-SPARK (Zhang et al., 2018). Reduced PKA enzymatic activity downstream of Rugose is consistent with functions as an A-Kinase Anchor Protein (AKAP; Wang et al., 2000; Volders et al., 2012), acting to regulate PKA localization and kinase activity (Smith et al., 2017). Consistently, Rugose and PKA catalytic subunit (PKA-C) interact in MB-dependent learning/memory (Zhao et al., 2013). Altering the FMRP-Rugose regulative mechanism in either direction drives F-actin assembly in the MB circuit, indicating a "Goldilocks zone" of optimal cytoskeleton control, consistent with known actin regulative dynamics (Niesmann et al., 2011). Increasing FMRP, Rugose or PKA-C function heightens F-actin assembly within the MB circuit. These findings reveal a new FMRP-Rugose-PKA mechanism regulating the neuronal actin cytoskeleton.

Conserved Rugose and Neurobeachin are both very large, brain-enriched AKAPs (Wang et al., 2000), although the AKAP function is unclear (Wild and Dell'Acqua, 2017). In general, AKAPs bind PKA to determine where, when and under what circumstances the kinase is activated (Smith et al., 2017; Wild and Dell'Acqua, 2017). In *Drosophila,* AKAP function is critical for aversive, but not appetitive, MB-dependent learning/memory (Schwaerzel et al., 2007). Consistently, PKA signaling is necessary for short-term memory formation mediated by the MB γ lobe (Zars et al., 2000; Blum et al., 2009; Qin et al., 2012), and the Rugose requirement in aversive learning/memory can be rescued by Rugose and Neurobeachin specifically targeted to the MB (Volders et al., 2012). Consistent with the focus of the current study, PKA signaling in the MB γ lobe has been argued to be particularly crucial for aversive short-term memory, and partial loss of Rugose and PKA-C interactively causes deficits in this memory performance (Zhao et al.,

2013). This mechanism is consistent with MB γ lobe actin cytoskeleton defects characterized in the current study. Taken together, the findings suggest Rugose AKAP misregulation of PKA activity in the FXS disease state impairs F-actin assembly dynamics in the MB γ lobe.

It is long-established that PKA signaling is necessary for MB-dependent learning (Davis and Dauwalder, 1991; Skoulakis et al., 1993; Lee and O'Dowd, 2000), with PKA signaling promoting activity-dependent plasticity in excitatory and inhibitory neurons (Wright and Zhong, 1995; Delgado et al., 1998; Ganguly and Lee, 2013; Lee, 2015). Moreover, in the FXS condition an excitatory/inhibitory imbalance has been reported at the circuit level, with both cell-autonomous reduced excitability and increased inhibition (Dahlhaus and El-Husseini, 2010; Olmos-Serrano et al., 2010; Doll and Broadie, 2014, 2016; Dahlhaus, 2018). Based on the current study, we find that MB Kenyon cells in the FXS condition exhibit a strongly reduced capacity for PKA signaling. We hypothesize that restoring PKA signaling capacity could correct actin cytoskeletal defects to enable Kenyon cell plasticity and MB circuit excitation/inhibition balance in the FXS model. Consequently, pharmacological interventions with phosphodiesterase (PDE) inhibitors, such as rolipram and Ro-20-1724 to increase cAMP signaling and PKA enzymatic activity (Kelley et al., 2007; Kanellopoulos et al., 2012; Choi et al., 2015), could prove effective in treating these FXS impairments.

It is reported that PDE inhibitors (e.g. rolipram) are insufficient to restore some FXS model MB behavioral defects (Androschuk et al., 2018), but can correct circuit-level defects. Thus, combinatorial strategies may be necessary to tackle the FXS/NBEA conditions. For example, in addition to correcting PKA signaling and F-actin dynamics, it may be required to also rectify *trans*-synaptic signaling and downstream signal transduction mechanisms (e.g. using minocycline and/or lithium) to restore the overall plastic responsivity of disease state neural circuits (Bilousova et al., 2008; Mines and Jope, 2011; Dear et al., 2017). In the future, we will also use optogenetic/odor activation of the MB circuitry (Doll et al., 2017) to test activity-dependent PKA signaling and F-actin cytoskeleton dynamics in both FXS and NBEA disease states, with and without PDE inhibitor pharmacological intervention. Furthermore, we will also aim to test PKA activity in neuron types throughout the MB circuit demonstrated to have altered activation states in the FXS model (Doll and Broadie, 2016; Doll et al., 2017). We hypothesize that differential PKA hyper- and hypo-activation in discrete neuron classes may be causative for excitation/inhibition circuit imbalance in FXS/NBEA conditions.

PKA-dependent effects on F-actin assembly dynamics is a likely mechanism for the well-characterized Kenyon cell overgrowth and lack of activity-dependent plasticity in the FXS model MB circuit (Pan et al., 2004; Tessier and Broadie, 2008; Doll and Broadie, 2015). Consistently, Rac1 activation with increased F- to G-actin is likewise reported in the FXS condition, with Rac1 changes driving neuronal morphology defects (Lee et al., 2003; Bongmba et al., 2011; Pyronneau et al., 2017). Although PKA effects on Rac1 are difficult to predict *in vivo* (Goto et al., 2014), our PKA-C gain-of-function results showing PKA activation promotes F-actin polymerization fit with Rac1 activation. We hypothesize that changes in Rac1 activation could account for increased F-actin assembly with both FMRP loss- and gain-of-function. However, several cytoskeletal regulators are disrupted in FXS models (Tessier and Broadie, 2012; Michaelsen-Preusse et al., 2018), for both microtubules (e.g. MAP1B/Futsch; Zhang et al., 2001; Wang et al., 2015) and F-actin (e.g. Profilin/Chickadee; Reeve et al., 2005). Thus, the mechanism revealed here is just part of a greater cytoskeleton dysfunction.

In conclusion, we report here defective FMRP-Rugose-PKA regulation of the neuronal actin cytoskeleton, consistent with neuronal structural defects characterizing FXS patients and disease models. Prior to this study, FXS patients and disease models were known to manifest striking cAMP signaling defects (Berry-Kravis and Huttenlocher, 1992; Berry-Kravis et al., 1995; Kelley et al., 2007), strongly suggesting altered PKA activity, but functional PKA enzymatic assays were lacking (Androschuk et al., 2018). To our knowledge, we are the first to confirm the hypothesis that PKA signaling is impaired in the FXS state, owing to the recent development of a beautiful PKA-SPARK transgenic *in vivo* activity sensor (Zhang et al., 2018). We discover here that FMRP promotes translation of Rugose/NBEA, a PKA-anchor specifically expressed in brain neurons (Wang et al., 2000; Volders et al., 2012), which in turn drives PKA activity regulating the neuronal actin cytoskeleton. Future experiments will explore the mechanistic link between PKA activation and F-actin dynamic regulation by using pharmacological and optogenetic manipulation of Rac1 function (Wu et al., 2009; Wang et al., 2010). This study links *Drosophila* FXS and NBEA disease models, providing a common pathway as a platform moving towards developing therapeutic treatments for related intellectual disability and autism spectrum disorders.

Conflict of interest

The authors declare no competing financial interests.

Acknowledgments

We are most grateful to Dr. Martin Schwärzel for *rugose* alleles and antibody, and Dr. Xiaokun Shu for the UAS-PKA-SPARK sensor line. We thank the Bloomington *Drosophila* Stock Center (Indiana University, USA) for *Drosophila* lines, and Developmental Studies Hybridoma Bank (University of Iowa, USA) for antibodies. We thank Broadie Lab members for input and Dominic Vita for expert advice. This work is supported by National Institutes of Health Grant MH084989 to K.B., and funding from Postdoctoral Training Program in Functional Neurogenomics (5T32MH065215) to J.S.

References

Abe, T., Yamazaki, D., Murakami, S., Hiroi, M., Nitta, Y., Maeyama, Y., Tabata, T., 2014. The NAV2 homolog Sickie regulates F-actin-mediated axonal growth in *Drosophila* mushroom body neurons via the non-canonical Rac-Cofilin pathway. Development 141, 4716–4728. https://doi.org/10.1242/dev.113308. (pmid: 25411210).

Androschuk, A., He, R.X., Weber, S., Rosenfelt, C., Bolduc, F.V., 2018. Stress odorant sensory response dysfunction in *Drosophila* Fragile X syndrome mutants. Front. Mol. Neurosci. 11, 242. https://doi.org/10.3389/fnmol.2018.00242. (pmid: 30135642).

Berry-Kravis, E., Huttenlocher, P.R., 1992. Cyclic AMP metabolism in fragile X syndrome. Ann. Neurol. 31, 22–26. https://doi.org/10.1002/ana.410310105. (pmid: 1371909).

Berry-Kravis, E., Hicar, M., Ciurlionis, R., 1995. Reduced cyclic AMP production in fragile X syndrome: cytogenetic and molecular correlations. Pediatr. Res. 38, 638–643. https://doi.org/10.1203/00006450-199511000-00002. (pmid: 8552427).

Bilousova, T.V., Dansie, L., Ngo, M., Aye, J., Charles, J.R., Ethell, D.W., Ethell, I.M., 2008. Minocycline promotes dendritic spine maturation and improves behavioural performance in the fragile X mouse model. J. Med. Genet. 46, 94–102. https://doi.org/10.1136/jmg.2008.061796. (pmid: 18835858).

Blum, A.L., Li, W., Cressy, M., Dubnau, J., 2009. Short- and long-term memory in *Drosophila* require cAMP signaling in distinct neuron types. Curr. Biol. 19, 1341–1350. https://doi.org/10.1016/j.cub.2009.07.016. (pmid: 19646879).

Bolduc, F.V., Bell, K., Cox, H., Broadie, K.S., Tully, T., 2008. Excess protein synthesis in *Drosophila* fragile X mutants impairs long-term memory. Nat. Neurosci. 11, 1143–1145. https://doi.org/10.1038/nn.2175. (pmid: 18776892).

Bongmba, O.Y.N., Martinez, L.A., Elhardt, M.E., Butler, K., Tejada-Simon, M.V., 2011. Modulation of dendritic spines and synaptic function by Rac1: A possible link to Fragile X syndrome pathology. Brain Res. 1399, 79–95. https://doi.org/10.1016/j.brainres.2011.05.020. (pmid: 21645877).

Castermans, D., Wilquet, V., Parthoens, E., Huysmans, C., Steyaert, J., Swinnen, L., Fryns, J.-P., Van de Ven, W., Devriendt, K., 2003. The neurobeachin gene is disrupted by a translocation in a patient with idiopathic autism. J. Med. Genet. 40, 352–356. https://doi.org/10.1136/jmg.40.5.352. (pmid: 12746398).

Castermans, D., Volders, K., Crepel, A., Backx, L., De Vos, R., Freson, K., Meulemans, S., Vermeesch, J.R., Schrander-Stumpel, C.T.R.M., De Rijk, P., Del-Favero, J., Van Geet, C., Van De Ven, W.J.M., Steyaert, J.G., Devriendt, K., Creemers, J.W.M., 2010. SCAMP5, NBEA and AMISYN: three candidate genes for autism involved in secretion of large dense-core vesicles. Hum. Mol. Genet. 19, 1368–1378. https://doi.org/10.1093/hmg/ddq013. (pmid: 20071347).

Choi, C.H., et al., 2015. PDE-4 inhibition rescues aberrant synaptic plasticity in *Drosophila* and mouse models of Fragile X syndrome. J. Neurosci. 35, 396–408. https://doi.org/10.1523/JNEUROSCI.1356-12.2015. (pmid: 25568131).

Cingolani, L.A., Goda, Y., 2008. Actin in action: the interplay between the actin cytoskeleton and synaptic efficacy. Nat. Rev. Neurosci. 9, 344–356. https://doi.org/10.1038/nrn2373. (pmid: 18425089).

Coffee, R.L., Tessier, C.R., Woodruff, E.A., Broadie, K., 2010. Fragile X mental retardation protein has a unique, evolutionarily conserved neuronal function not shared with

FXR1P or FXR2P. Dis. Model Mech. 3, 471–485. https://doi.org/10.1242/dmm.004598. (pmid: 20442204).
Coffee, R.L., Williamson, A.J., Adkins, C.M., Gray, M.C., Page, T.L., Broadie, K., 2012. *In vivo* neuronal function of the fragile X mental retardation protein is regulated by phosphorylation. Hum. Mol. Genet. 21, 900–915. https://doi.org/10.1093/hmg/ddr527. (pmid: 22080836).
Comery, T.A., Harris, J.B., Willems, P.J., Oostra, B.A., Irwin, S.A., Weiler, I.J., Greenough, W.T., 1997. Abnormal dendritic spines in fragile X knockout mice: maturation and pruning deficits. Proc. Natl. Acad. Sci. 94, 5401–5404. https://doi.org/10.1073/pnas.94.10.5401. (pmid: 9144249).
Connolly, J.B., Roberts, I.J., Armstrong, J.D., Kaiser, K., Forte, M., Tully, T., O'Kane, C.J., 1996. Associative learning disrupted by impaired Gs signaling in Drosophila mushroom bodies. Science 274, 2104–2107. https://doi.org/10.1126/science.274.5295.2104. (pmid: 8953046).
Crittenden, J.R., Skoulakis, E.M.C., Han, K.A., Kalderon, D., Davis, R.L., 1998. Tripartite mushroom body architecture revealed by antigenic markers. Learn. Mem. 5, 38–51 (pmid: 10454371).
Dahlhaus, R., 2018. Of men and mice: modeling the Fragile X Syndrome. Front. Mol. Neurosci. 11, 41. https://doi.org/10.3389/fnmol.2018.00041. (pmid: 29599705).
Dahlhaus, R., El-Husseini, A., 2010. Altered neuroligin expression is involved in social deficits in a mouse model of the fragile X syndrome. Behav. Brain Res. 208, 96–105. https://doi.org/10.1016/j.bbr.2009.11.019. (pmid: 19932134).
Darnell, J.C., Van Driesche, S.J., Zhang, C., Hung, K.Y.S., Mele, A., Fraser, C.E., Stone, E.F., Chen, C., Fak, J.J., Chi, S.W., Licatalosi, D.D., Richter, J.D., Darnell, R.B., 2011. FMRP stalls ribosomal translocation on mRNAs linked to synaptic function and autism. Cell 146, 247–261. https://doi.org/10.1016/j.cell.2011.06.013. (pmid: 21784246).
Davis, J.K., Broadie, K., 2017. Multifarious Functions of the Fragile X Mental Retardation Protein. Trends Genet 33, 703–714. https://doi.org/10.1016/j.tig.2017.07.008. (pmid: 28826631).
Davis, R.L., Dauwalder, B., 1991. The *Drosophila dunce* locus: learning and memory genes in the fly. Trends Genet. 7, 224–229. https://doi.org/10.1016/0168-9525(91)90369-2. (pmid: 1653476).
Dear, M.L., Shilts, J., Broadie, K., 2017. Neuronal activity drives FMRP- and HSPG-dependent matrix metalloproteinase function required for rapid synaptogenesis. Sci. Signal. 10https://doi.org/10.1126/scisignal.aan3181. eaan3181. (pmid: 29114039).
Delgado, R., Davis, R., Bono, M.R., Latorre, R., Labarca, P., 1998. Outward currents in Drosophila larval neurons: dunce lacks a maintained outward current component downregulated by cAMP. J. Neurosci. 18, 1399–1407. https://doi.org/10.1523/JNEUROSCI.18-04-01399.1998. (pmid:9454849).
Derlig, K., Gießl, A., Brandstätter, J.H., Enz, R., Dahlhaus, R., 2013. Identification and characterisation of simiate, a novel protein linked to the fragile X syndrome. PLoS One 8, e83007. https://doi.org/10.1371/journal.pone.0083007. (pmid: 24349419).
Derlig, K., Ehrhardt, T., Gießl, A., Brandstätter, J.H., Enz, R., Dahlhaus, R., 2014. Simiate is an Actin binding protein involved in filopodia dynamics and arborization of neurons. Front Cell Neurosci. 8, 99. https://doi.org/10.3389/fncel.2014.00099. (pmid: 24782708).
Doll, C.A., Broadie, K., 2014. Impaired activity-dependent neural circuit assembly and refinement in autism spectrum disorder genetic models. Front. Cell Neurosci. 8, 30. https://doi.org/10.3389/fncel.2014.00030. (pmid: 24570656).
Doll, C.A., Broadie, K., 2015. Activity-dependent FMRP requirements in development of the neural circuitry of learning and memory. Development 142, 1346–1356. https://doi.org/10.1242/dev.117127. (pmid: 25804740).
Doll, C.A., Broadie, K., 2016. Neuron class-specific requirements for Fragile X Mental Retardation Protein in critical period development of calcium signaling in learning and memory circuitry. Neurobiol. Dis. 89, 76–87. https://doi.org/10.1016/j.nbd.2016.02.006. (pmid: 26851502).
Doll, C.A., Vita, D.J., Broadie, K., 2017. Fragile X mental retardation protein requirements in activity-dependent critical period neural circuit refinement. Curr. Biol. 27, 2318–2330. https://doi.org/10.1016/j.cub.2017.06.046. (pmid: 28756946).
Durocher, D., Taylor, I.A., Sarbassova, D., Haire, L.F., Westcott, S.L., Jackson, S.P., Smerdon, S.J., Yaffe, M.B., 2000. The molecular basis of FHA domain:phosphopeptide binding specificity and implications for phospho-dependent signaling mechanisms. Mol. Cell 6, 1169–1182. https://doi.org/10.1016/S1097-2765(00)00114-3. (pmid: 11106755).
Eaton, S.L., Roche, S.L., Llavero Hurtado, M., Oldknow, K.J., Farquharson, C., Gillingwater, T.H., Wishart, T.M., 2013. Total protein analysis as a reliable loading control for quantitative fluorescent Western blotting. PLoS One 8, e72457. https://doi.org/10.1371/journal.pone.0072457. (pmid: 24023619).
Fouquet, W., Owald, D., Wichmann, C., Mertel, S., Depner, H., Dyba, M., Hallermann, S., Kittel, R.J., Eimer, S., Sigrist, S.J., 2009. Maturation of active zone assembly by Drosophila Bruchpilot. J. Cell Biol. 186, 129–145. https://doi.org/10.1083/jcb.200812150. (pmid: 19596851).
Ganguly, A., Lee, D., 2013. Suppression of inhibitory GABAergic transmission by cAMP signaling pathway: alterations in learning and memory mutants. Eur. J. Neurosci. 37, 1383–1393. https://doi.org/10.1111/ejn.12144. (pmid: 23387411).
Gatto, C.L., Broadie, K., 2009. Temporal requirements of the fragile x mental retardation protein in modulating circadian clock circuit synaptic architecture. Front. Neural Circuits 3, 8. https://doi.org/10.3389/neuro.04.008.2009. (pmid: 19738924).
Goto, A., Kamioka, Y., Matsuda, M., 2014. PKA modulation of Rac in neuronal cells. Front Cell Neurosci. 8, 8–11. https://doi.org/10.3389/fncel.2014.00321. (pmid: 25352782).
Greenblatt, E.J., Spradling, A.C., 2018. Fragile X mental retardation 1 gene enhances the translation of large autism-related proteins. Science 361, 709–712. https://doi.org/10.1126/science.aas9963. (pmid: 30115809).
Gromova, K.V., Muhia, M., Rothammer, N., Gee, C.E., Thies, E., Schaefer, I., Kress, S., Kilimann, M.W., Shevchuk, O., Oertner, T.G., Kneussel, M., 2018. Neurobeachin and the kinesin KIF21B Are critical for endocytic recycling of NMDA receptors and regulate social behavior. Cell Rep. 23, 2705–2717. https://doi.org/10.1016/j.celrep.2018.04.112. (pmid: 29847800).
Huelsmann, S., Ylänne, J., Brown, N.H., 2013. Filopodia-like actin cables position nuclei in association with perinuclear actin in Drosophila nurse cells. Dev. Cell 26, 604–615. https://doi.org/10.1016/j.devcel.2013.08.014. (pmid: 24091012).
Hunter, J., Rivero-Arias, O., Angelov, A., Kim, E., Fotheringham, I., Leal, J., 2014. Epidemiology of fragile X syndrome: a systematic review and meta-analysis. Am. J. Med. Genet. A 164A, 1648–1658. https://doi.org/10.1002/ajmg.a.36511. (pmid: 24700618).
Jacquemont, S., Pacini, L., Jønch, A.E., Cencelli, G., Rozenberg, I., He, Y., D'Andrea, L., Pedini, G., Eldeeb, M., Willemsen, R., Gasparini, F., Tassone, F., Hagerman, R., Gomez-Mancilla, B., Bagni, C., 2018. Protein synthesis levels are increased in a subset of individuals with fragile X syndrome. Hum. Mol. Genet. 27, 2039–2051. https://doi.org/10.1093/hmg/ddy099. (pmid: 29590342).
Jenett, A., et al., 2012. A GAL4-driver line resource for Drosophila neurobiology. Cell Rep. 2, 991–1001. https://doi.org/10.1016/j.celrep.2012.09.011. (pmid: 23063364).
Kanellopoulos, A.K., Semelidou, O., Kotini, A.G., Anezaki, M., Skoulakis, E.M.C., 2012. Learning and memory deficits consequent to reduction of the fragile X mental retardation protein result from metabotropic glutamate receptor-mediated inhibition of cAMP signaling in *Drosophila*. J. Neurosci. 32, 13111–13124. https://doi.org/10.1523/JNEUROSCI.1347-12.2012. (pmid: 22993428).
Kashima, R., Redmond, P.L., Ghatpande, P., Roy, S., Kornberg, T.B., Hanke, T., Knapp, S., Lagna, G., Hata, A., 2017. Hyperactive locomotion in a *Drosophila* model is a functional readout for the synaptic abnormalities underlying fragile X syndrome. Sci. Signal. 10https://doi.org/10.1126/scisignal.aai8133. eaai8133. (pmid: 28465421).
Kelley, D.J., Davidson, R.J., Elliott, J.L., Lahvis, G.P., Yin, J.C.P., Bhattacharyya, A., 2007. The cyclic AMP cascade is altered in the fragile X nervous system. PLoS One 2, e931. https://doi.org/10.1371/journal.pone.0000931. (pmid: 17895972).
Kiger, J.A., O'Shea, C., 2001. Genetic evidence for a protein kinase A/cubitus interruptus complex that facilitates processing of cubitus interruptus in *Drosophila*. Genetics 158, 1157–1166 (pmid: 11454764).
Kiger, J.A., Eklund, J.L., Younger, S.H., O'Kane, C.J., 1999. Transgenic inhibitors identify two roles for protein kinase A in *Drosophila* development. Genetics 152, 281–290 (pmid: 10224260).
Laggerbauer, B., Ostareck, D., Keidel, E.M., Ostareck-Lederer, A., Fischer, U., 2001. Evidence that fragile X mental retardation protein is a negative regulator of translation. Hum. Mol. Genet. 10, 329–338. https://doi.org/10.1093/hmg/10.4.329. (pmid: 11157796).
Lee, D., 2015. Global and local missions of cAMP signaling in neural plasticity, learning, and memory. Front. Pharmacol. 6, 161. https://doi.org/10.3389/fphar.2015.00161. (pmid: 26300775).
Lee, D., O'Dowd, D.K., 2000. cAMP-dependent plasticity at excitatory cholinergic synapses in *Drosophila* neurons: alterations in the memory mutant *dunce*. J. Neurosci. 20, 2104–2111. https://doi.org/10.1523/JNEUROSCI.20-06-02104.2000. (pmid: 10704484).
Lee, A., Li, W., Xu, K., Bogert, B.A., Su, K., Gao, F.-B., 2003. Control of dendritic development by the *Drosophila* fragile X-related gene involves the small GTPase Rac1. Development 130, 5543–5552. https://doi.org/10.1242/dev.00792. (pmid: 14530299).
Li, Z., Zhang, Y., Ku, L., Wilkinson, K.D., Warren, S.T., Feng, Y., 2001. The fragile X mental retardation protein inhibits translation via interacting with mRNA. Nucleic Acids Res. 29, 2276–2283. https://doi.org/10.1093/nar/29.11.2276. (pmid: 11376146).
Lin, B., Kramár, E.A., Bi, X., Brucher, F.A., Gall, C.M., Lynch, G., 2005. Theta stimulation polymerizes actin in dendritic spines of hippocampus. J. Neurosci. 25, 2062–2069. https://doi.org/10.1523/JNEUROSCI.4283-04.2005. (pmid: 15728846).
Melak, M., Plessner, M., Grosse, R., 2017. Actin visualization at a glance. J Cell Sci. 130, 525–530. https://doi.org/10.1242/jcs.189068. (pmid: 28082420).
Michaelsen-Preusse, K., Feuge, J., Korte, M., 2018. Imbalance of synaptic actin dynamics as a key to fragile X syndrome? J. Physiol. 596, 2773–2782. https://doi.org/10.1113/JP275571. (pmid: 29380377).
Mines, M.A., Jope, R.S., 2011. Glycogen synthase kinase-3: a promising therapeutic target for fragile x syndrome. Front. Mol. Neurosci. 4, 35. https://doi.org/10.3389/fnmol.2011.00035. (pmid: 22053151).
Nair, R., Lauks, J., Jung, S., Cooke, N.E., de Wit, H., Brose, N., Kilimann, M.W., Verhage, M., Rhee, J., 2013. Neurobeachin regulates neurotransmitter receptor trafficking to synapses. J. Cell Biol. 200, 61–80. https://doi.org/10.1083/jcb.201207113. (pmid: 23277425).
Niesmann, K., Breuer, D., Brockhaus, J., Born, G., Wolff, I., Reissner, C., Kilimann, M.W., Rohlmann, A., Missler, M., 2011. Dendritic spine formation and synaptic function require neurobeachin. Nat. Commun. 2, 557. https://doi.org/10.1038/ncomms1565. (pmid: 22109531).
Nuytens, K., Gantois, I., Stijnen, P., Iscru, E., Laeremans, A., Serneels, L., Van Eylen, L., Liebhaber, S.A., Devriendt, K., Balschun, D., Arckens, L., Creemers, J.W.M., D'Hooge, R., 2013. Haploinsufficiency of the autism candidate gene Neurobeachin induces autism-like behaviors and affects cellular and molecular processes of synaptic plasticity in mice. Neurobiol. Dis. 51, 144–151. https://doi.org/10.1016/j.nbd.2012.11.004. (pmid: 23153818).
Olmos-Serrano, J.L., Paluszkiewicz, S.M., Martin, B.S., Kaufmann, W.E., Corbin, J.G., Huntsman, M.M., 2010. Defective GABAergic Neurotransmission and Pharmacological Rescue of Neuronal Hyperexcitability in the Amygdala in a Mouse Model of Fragile X Syndrome. J. Neurosci. 30, 9929–9938. https://doi.org/10.1523/JNEUROSCI.1714-10.2010. (pmid: 20660275).

Pan, L., Zhang, Y.Q., Woodruff, E., Broadie, K., 2004. The *Drosophila* fragile X gene negatively regulates neuronal elaboration and synaptic differentiation. Curr. Biol. 14, 1863–1870. https://doi.org/10.1016/j.cub.2004.09.085. (pmid: 15498496).

Pyronneau, A., He, Q., Hwang, J., Porch, M., Contractor, A., Zukin, R.S., 2017. Aberrant Rac1-cofilin signaling mediates defects in dendritic spines, synaptic function, and sensory perception in fragile X syndrome. Sci. Signal. 10, 1–16. https://doi.org/10.1126/scisignal.aan0852. (pmid: 29114038).

Qin, H., Cressy, M., Li, W., Coravos, J.S., Izzi, S.A., Dubnau, J., 2012. Gamma neurons mediate dopaminergic input during aversive olfactory memory formation in Drosophila. Curr. Biol. 22, 608–614. https://doi.org/10.1016/j.cub.2012.02.014. (pmid: 22425153).

Reeve, S.P., Bassetto, L., Genova, G.K., Kleyner, Y., Leyssen, M., Jackson, F.R., Hassan, B.A., 2005. The Drosophila fragile X mental retardation protein controls actin dynamics by directly regulating profilin in the brain. Curr. Biol. 15, 1156–1163. https://doi.org/10.1016/j.cub.2005.05.050. (pmid: 15964283).

Schiffhauer, E.S., Luo, T., Mohan, K., Srivastava, V., Qian, X., Griffis, E.R., Iglesias, P.A., Robinson, D.N., 2016. Mechanoaccumulative elements of the mammalian actin cytoskeleton. Curr. Biol. 26, 1473–1479. https://doi.org/10.1016/j.cub.2016.04.007. (pmid: 27185555).

Schwaerzel, M., Jaeckel, A., Mueller, U., 2007. Signaling at A-kinase anchoring proteins organizes anesthesia-sensitive memory in *Drosophila*. J. Neurosci. 27, 1229–1233. https://doi.org/10.1523/JNEUROSCI.4622-06.2007. (pmid: 17267579).

Sears, J.C., Broadie, K., 2018. Fragile X mental retardation protein regulates activity-dependent membrane trafficking and *trans*-synaptic signaling mediating synaptic remodeling. Front. Mol. Neurosci. 10, 440. https://doi.org/10.3389/fnmol.2017.00440. (pmid: 29375303).

Skoulakis, E.M.C., Kalderon, D., Davis, R.L., 1993. Preferential expression in mushroom bodies of the catalytic subunit of protein kinase A and its role in learning and memory. Neuron 11, 197–208. https://doi.org/10.1016/0896-6273(93)90178-T. (pmid: 8352940).

Smith, F.D., Esseltine, J.L., Nygren, P.J., Veesler, D., Byrne, D.P., Vonderach, M., Strashnov, I., Eyers, C.E., Eyers, P.A., Langeberg, L.K., Scott, J.D., 2017. Local protein kinase A action proceeds through intact holoenzymes. Science 356, 1288–1293. https://doi.org/10.1126/science.aaj1669. (pmid: 28642438).

Tessier, C.R., Broadie, K., 2008. *Drosophila* fragile X mental retardation protein developmentally regulates activity-dependent axon pruning. Development 135, 1547–1557. https://doi.org/10.1242/dev.015867. (pmid: 18321984).

Tessier, C.R., Broadie, K., 2011. The fragile X mental retardation protein developmentally regulates the strength and fidelity of calcium signaling in *Drosophila* mushroom body neurons. Neurobiol. Dis. 41, 147–159. https://doi.org/10.1016/j.nbd.2010.09.002. (pmid: 20843478).

Tessier, C.R., Broadie, K., 2012. Molecular and genetic analysis of the Drosophila model of fragile X syndrome. In: Denman, R.B. (Ed.), Modeling Fragile X syndrome. Results and Problems in Cell Differentiation *Springer*, Berlin Heidelberg, pp. 119–156. https://doi.org/10.1007/978-3-642-21649-7_7. (pmid: 22009350).

Todd, P.K., Mack, K.J., Malter, J.S., 2003. The fragile X mental retardation protein is required for type-I metabotropic glutamate receptor-dependent translation of PSD-95. Proc. Natl. Acad. Sci. 100, 14374–14378. https://doi.org/10.1073/pnas.2336265100. (pmid: 14614133).

Vasmer, D., 2016. Morphological Analysis of Kenyon Cells of the *Drosophila* Mushroom Bodies. PhD Dissertation. Unniversity of Göttingen. https://ediss.uni-goettingen.de.

Verkerk, A.J., Pieretti, M., Sutcliffe, J.S., Fu, Y.H., Kuhl, D.P., Pizzuti, A., Reiner, O., Richards, S., Victoria, M.F., Zhang, F.P., 1991. Identification of a gene (FMR-1) containing a CGG repeat coincident with a breakpoint cluster region exhibiting length variation in fragile X syndrome. Cell 65, 905–914. https://doi.org/10.1016/0092-8674(91)90397-H. (pmid: 1710175).

Vita, D.J., Broadie, K., 2017. ESCRT-III membrane trafficking misregulation contributes to fragile X syndrome synaptic defects. Sci. Rep. 7, 8683. https://doi.org/10.1038/s41598-017-09103-6. (pmid: 28819289).

Volders, K., Scholz, S., Slabbaert, J.R., Nagel, A.C., Verstreken, P., Creemers, J.W.M., Callaerts, P., Schwärzel, M., 2012. *Drosophila rugose* is a functional homolog of mammalian *Neurobeachin* and affects synaptic architecture, brain morphology, and associative learning. J. Neurosci. 32, 15193–15204. https://doi.org/10.1523/JNEUROSCI.6424-11.2012. (pmid: 23100440).

Wan, L., Dockendorff, T.C., Jongens, T.A., Dreyfuss, G., 2000. Characterization of dFMR1, a *Drosophila melanogaster* homolog of the fragile X mental retardation protein. Mol. Cell Biol. 20, 8536–8547. https://doi.org/10.1128/MCB.20.22.8536-8547.2000. (pmid: 11046149).

Wang, X., Herberg, F.W., Laue, M.M., Wullner, C., Hu, B., Petrasch-Parwez, E., Kilimann, M.W., 2000. Neurobeachin: A protein kinase A-anchoring, beige/Chediak-higashi protein homolog implicated in neuronal membrane traffic. J. Neurosci. 20, 8551–8565. https://doi.org/10.1523/JNEUROSCI.20-23-08551.2000. (pmid: 11102458).

Wang, X., He, L., Wu, Y.I., Hahn, K.M., Montell, D.J., 2010. Light-mediated activation reveals a key role for Rac in collective guidance of cell movement *in vivo*. Nat. Cell Biol. 12, 591–597. https://doi.org/10.1038/ncb2061. (pmid: 20473296).

Wang, B., Pan, L., Wei, M., Wang, Q., Liu, W.-W., Wang, N., Jiang, X.-Y., Zhang, X., Bao, L., 2015. FMRP-mediated axonal delivery of miR-181d regulates axon elongation by locally targeting Map1b and Calm1. Cell Rep. 13, 2794–2807. https://doi.org/10.1016/j.celrep.2015.11.057. (pmid: 26711345).

Wild, A.R., Dell'Acqua, M.L., 2017. Potential for therapeutic targeting of AKAP signaling complexes in nervous system disorders. Pharmacol. Ther. 185, 99–121. https://doi.org/10.1016/j.pharmthera.2017.12.004. (pmid: 29262295).

Woolfson, D.N., Bartlett, G.J., Burton, A.J., Heal, J.W., Niitsu, A., Thomson, A.R., Wood, C.W., 2015. *De novo* protein design: how do we expand into the universe of possible protein structures? Curr. Opin. Struct. Biol. 33, 16–26. https://doi.org/10.1016/j.sbi.2015.05.009. (pmid: 26093060).

Wright, N.J., Zhong, Y., 1995. Characterization of K+ currents and the cAMP-dependent modulation in cultured *Drosophila* mushroom body neurons identified by lacZ expression. J. Neurosci. 15, 1025–1034. https://doi.org/10.1523/JNEUROSCI.15-02-01025.1995. (pmid:7869080).

Wu, Y.I., Frey, D., Lungu, O.I., Jaehrig, A., Schlichting, I., Kuhlman, B., Hahn, K.M., 2009. A genetically encoded photoactivatable Rac controls the motility of living cells. Nature 461, 104–108. https://doi.org/10.1038/nature08241. (pmid: 19693014).

Zalfa, F., Giorgi, M., Primerano, B., Moro, A., Di Penta, A., Reis, S., Oostra, B., Bagni, C., 2003. The Fragile X syndrome protein FMRP associates with BC1 RNA and regulates the translation of specific mRNAs at synapses. Cell 112, 317–327. https://doi.org/10.1016/S0092-8674(03)00079-5. (pmid: 12581522).

Zars, T., Fischer, M., Schulz, R., Heisenberg, M., 2000. Localization of a short-term memory in *Drosophila*. Science 288, 672–675. https://doi.org/10.1126/science.288.5466.672. (pmid: 10784450).

Zhang, Y.Q., Bailey, A.M., Matthies, H.J.G., Renden, R.B., Smith, M.A., Speese, S.D., Rubin, G.M., Broadie, K., 2001. *Drosophila* Fragile X-Related Gene Regulates the MAP1B Homolog Futsch to Control Synaptic Structure and Function. Cell 107, 591–603. https://doi.org/10.1016/S0092-8674(01)00589-X. (pmid: 11733059).

Zhang, Q., Huang, H., Zhang, L., Wu, R., Chung, C.-I., Zhang, S.-Q., Torra, J., Schepis, A., Coughlin, S.R., Kornberg, T.B., Shu, X., 2018. Visualizing dynamics of cell signaling *in vivo* with a phase separation-based kinase reporter. Mol. Cell 69, 334–346. https://doi.org/10.1016/j.molcel.2017.12.008. e4 (pmid: 29307513).

Zhao, J., Lu, Y., Zhao, X., Yao, X., Shuai, Y., Huang, C., Wang, L., Jeong, S.H., Zhong, Y., 2013. Dissociation of *rugose*-dependent short-term memory component from memory consolidation in *Drosophila*. Genes Brain Behav. 12, 626–632. https://doi.org/10.1111/gbb.12056. (pmid: 23790035).

Zhu, G., Liu, Y., Wang, Y., Bi, X., Baudry, M., 2015. Different patterns of electrical activity lead to long-term potentiation by activating different intracellular pathways. J. Neurosci. 35, 621–633. https://doi.org/10.1523/JNEUROSCI.2193-14.2015. (pmid: 25589756).